

1 **Title: CA2 Neuronal Activity Controls Hippocampal Oscillations and Social**
2 **Behavior**

3
4 Authors: Georgia M. Alexander¹, Logan Y. Brown¹, Shannon Farris¹, Daniel
5 Lustberg¹, Caroline Pantazis², Bernd Gloss¹, Nicholas W. Plummer¹, Natallia V.
6 Riddick³, Sheryl S. Moy³, Patricia Jensen¹, Serena M. Dudek^{1*}

7
8 ¹ Neurobiology Laboratory, National Institute of Environmental Health Sciences,
9 National Institutes of Health, 111 T.W. Alexander Drive, Mail Drop F2-04
10 Research Triangle Park, North Carolina 27709, USA

11 ² Brain Health Institute, Rutgers University, Piscataway, NJ 08854, USA

12 ³ Carolina Institute for Developmental Disabilities and Department of Psychiatry,
13 University of North Carolina School of Medicine, 111 Mason Farm Road, Chapel
14 Hill, NC 27599, USA

15 * Corresponding Author and Lead Contact: dudek@niehs.nih.gov

16
17 **RUNNING TITLE:** Gamma oscillations in CA2

18
19 **KEYWORDS:** Hippocampal CA2; DREADD; hM3Dq; hM4Di; Gamma Oscillation;
20 Ripple; Prefrontal Cortex; Social Behavior; In Vivo Electrophysiology

21
22 **Abstract**

23
24 Hippocampal oscillations arise from coordinated activity among distinct
25 populations of neurons and are associated with cognitive functions and
26 behaviors. Although much progress has been made toward identifying the
27 relative contribution of specific neuronal populations in hippocampal oscillations,
28 far less is known about the role of hippocampal area CA2, which is thought to
29 support social aspects of episodic memory. Furthermore, the little existing
30 evidence on the role of CA2 in oscillations have led to conflicting conclusions.
31 Therefore, we sought to identify the specific contribution of CA2 pyramidal
32 neurons to brain oscillations using a controlled experimental system. We used
33 excitatory and inhibitory DREADDs in transgenic mice to acutely and reversibly
34 manipulate CA2 pyramidal cell activity. Here, we report on the role of CA2 in
35 hippocampal-prefrontal cortical network oscillations and social behavior. We
36 found that excitation or inhibition of CA2 pyramidal cell activity bidirectionally
37 regulated hippocampal and prefrontal cortical low gamma oscillations and
38 inversely modulated hippocampal ripple oscillations. Further, CA2 inhibition
39 impaired social approach behavior. These findings support a role for CA2 in low
40 gamma generation and ripple modulation within the hippocampus and
41 underscore the importance of CA2 neuronal activity in extrahippocampal
42 oscillations and social behavior.

43
44

45 Area CA2 of the hippocampus has become appreciated as a distinct subfield of
46 hippocampus based on several molecular, synaptic, anatomical, and functional
47 properties (see¹ for review). We and others have recently identified similarities
48 and differences between CA2 and the neighboring CA1 and CA3 subfields based
49 on action potential firing *in vivo*²⁻⁶. In addition to action potential firing, another
50 form of neuronal communication is achieved through synchronized oscillations,
51 which reflect the summated electrical activity of a population of neurons and can
52 be detected in local field potentials (LFPs). CA1 and CA3 networks propagate
53 oscillations in three primary frequency bands: theta (~5-10 Hz), gamma (~30-100
54 Hz) and sharp-wave ripples (~100-250 Hz). A few studies have reported
55 properties of network oscillations in CA2⁶⁻⁸, but none of them have examined
56 CA2 gamma oscillations or the impact of CA2 oscillations on extrahippocampal
57 structures.

58
59 In the hippocampus, high and low gamma oscillations are thought to arise from
60 two distinct sources and likely play separate roles in memory⁹. High gamma
61 (~60-100 Hz) oscillations in CA1 are prevalent in stratum lacunosum-
62 moleculare¹⁰, co-occur with high gamma oscillations in medial entorhinal cortex
63 (MEC)⁹, and are impaired by lesioning of EC¹¹, leading to the conclusion that
64 high gamma oscillations arise from MEC. High gamma is thought to contribute to
65 memory encoding because high gamma power is increased upon exploration of
66 novel stimuli^{12,13}. Low gamma (~30-55 Hz) oscillations in CA1 are prevalent in
67 stratum radiatum¹⁰, synchronize with low gamma in CA3¹⁴, and become more
68 evident upon EC lesioning¹¹, supporting the conclusion that low gamma
69 oscillations arise from CA3. Low gamma oscillations are believed to promote
70 memory retrieval because the magnitude of low gamma coupling to theta
71 oscillations correlates with performance on learned behavioral tasks^{15,16}.
72 Interestingly, complete silencing of the synaptic output of CA3 with tetanus toxin
73 light chain does not completely impair low gamma oscillations¹⁷, suggesting the
74 presence of another source of low gamma oscillations.

75
76 Another prominent oscillation seen in hippocampus is sharp-wave ripple
77 oscillations, which are high frequency (~100-250 Hz), short-duration electrical
78 events prominently seen in LFP recordings from CA1 during awake immobility
79 and slow wave sleep¹⁸. Sharp waves are thought to arise from the synchronous
80 firing of CA3 pyramidal cells, which depolarizes the apical dendrites of CA1
81 pyramidal cells. The synchronous CA3 firing recruits excitatory and inhibitory
82 neurons in CA1 to generate ripples^{18,19}. A role for CA2 neurons in sharp-wave
83 ripples has recently been suggested based on three *in vivo* electrophysiology
84 studies⁶⁻⁸, although consensus has not been reached on the precise role that
85 these neurons play. Kay et al. found that CA2 is the only hippocampal subregion
86 to have a substantial population of neurons that cease firing during ripples
87 (termed 'N cells'), whereas nearly all pyramidal cells queried in neighboring
88 subfields fired during ripples. Although not associated with ripples, these N cells
89 fired at high rates during low running speed or immobility⁶. Oliva et al. later
90 reported that CA2 pyramidal cell activity ramps up before the onset of sharp-

91 wave ripples, leading these authors to conclude that CA2 neurons play a leading
92 role in ripple generation. By contrast, Boehringer et al. later found that chronic
93 silencing of CA2 pyramidal cell output leads to the occurrence of epileptic
94 discharges arising from CA3, which the authors suggested reflect anomalous
95 ripple oscillations. Accordingly, findings of the Boehringer study do not appear to
96 support the conclusion of Oliva et al. that CA2 neurons initiate ripples. Given the
97 disparate conclusions of these reports, further study is required to clarify the role
98 of CA2 neuronal activity in ripple generation.

99
100 Area CA2 has recently been recognized for its role in processing long term
101 memories containing socially relevant information in rodents^{2,20-22}. Interestingly, a
102 mouse model of schizophrenia that shows hypoactive CA2 pyramidal cells *in*
103 *vitro* also shows impaired social behavior²³. Further, long range synchrony
104 between hippocampus and prefrontal cortex (PFC), including low gamma
105 coherence, is impaired in another mouse model of schizophrenia²⁴, raising the
106 question of how altering CA2 pyramidal cell activity experimentally may impact
107 social behavior and synchrony between hippocampus and PFC.

108
109 In this study, we present evidence that selective, acute activation or inhibition of
110 CA2 pyramidal cells using Cre-dependent expression of Gq- and Gi-coupled
111 DREADD receptors (hM3Dq and hM4Di^{25,26}, respectively) bidirectionally
112 modulates low gamma oscillations in both hippocampus and PFC and ripple
113 occurrence in hippocampus. Further, manipulation of CA2 with the inhibitory
114 DREADD affected behavior in one measurement of social function.

115

116 RESULTS

117

118 **Increasing CA2 pyramidal cell activity increases hippocampal and** 119 **prefrontal cortical low gamma power.**

120 To gain selective genetic access to molecularly-defined CA2, we generated a
121 tamoxifen-inducible mouse line, *Amigo2-icreERT2*. When combined with a Cre-
122 dependent tdTomato reporter mouse line²⁷, we observed robust expression of
123 tdTomato in CA2 of brain sections from *Amigo2-icreERT2+; ROSA-tdTomato+/-*
124 mice treated with tamoxifen. Expression of tdTomato colocalized with the CA2
125 pyramidal cell marker, PCP4²⁸, in 91.4% of neurons (N=6 mice; Fig. S1), and
126 tdTomato colocalized with a marker of hippocampal pyramidal neurons (N=6; Fig
127 S1, S2) but not inhibitory neurons (N=3; Fig S1, S2). Expression of tdTomato
128 was also observed in extra-hippocampal brain structures and associated with
129 vasculature. In control experiments, *Amigo2-icreERT2+; ROSA-tdTomato+/-*
130 animals treated with corn oil (the tamoxifen vehicle) showed no tdTomato
131 expression (N=3; Fig. S3).

132

133 Infusion of AAVs encoding Cre-dependent hM3Dq (Fig. 1A-C, E) or hM4Di (Fig.
134 1D) with the neuron-specific human synapsin promoter into *Amigo2-icreERT2+*
135 mice allowed for selective expression of mCherry-DREADD in CA2 pyramidal
136 neurons without expression in fasciola cinerea, outside of the hippocampus, or in

137 the vasculature, as detected by co-expression of mCherry with PCP4 (N=4; Fig
138 1A-B, E). Expression of mCherry also colocalized with the pyramidal cell marker,
139 CaMKII α (N=4; Fig. 1C, Fig. S2), but not the interneuron marker, glutamic acid
140 decarboxylase (GAD) in *GAD-eGFP+*; *Amigo2-icreERT2+* mice (N=4; Fig. 1D,
141 Fig. S2). In control *Amigo2-icreERT2-* mice infused with hM3Dq AAV, mCherry
142 expression was absent (N=4; Fig. S3).

143

144 With genetic access to CA2 pyramidal cells gained, we could selectively modify
145 activity of CA2 neurons *in vivo* with excitatory or inhibitory DREADDs and
146 measure the resulting network and behavioral effects. One advantage of
147 DREADDs is that compared with tetanus toxin light chain, which permanently
148 silences neuronal output, DREADDs permit transient modification of neuronal
149 activity (between 4 and 24 hours; see also Fig. S9), reducing the potential for
150 compensatory circuit reorganization.

151

152 To measure the effect of increasing CA2 neuronal activity on hippocampal and
153 prefrontal cortical population oscillatory activity, *Amigo2-icreERT2+* and control
154 *Amigo2-icreERT2-* mice were infused unilaterally with hM3Dq AAV, treated with
155 tamoxifen and then implanted with electrodes in hippocampus and PFC (see Fig.
156 S4). To confirm that hM3Dq increased neuronal activity, single-unit firing rate
157 was measured from CA2/proximal CA1 pyramidal neurons. CNO treatment dose-
158 dependently increased the firing rate of pyramidal neurons following CNO
159 administration (Fig. S5). Next, *Amigo2-icreERT2+* and control *Amigo2-icreERT2-*
160 mice were treated with various doses of CNO or vehicle as control, and
161 hippocampal LFPs were assessed for CNO treatment-dependent effects using
162 spectral analyses, focusing on theta (5-10 Hz), beta (14-18 Hz) low gamma (30-
163 60 Hz) and high gamma (65-100 Hz) oscillations. We measured oscillatory power
164 during the 30 to 60 min time window following treatment during each of running
165 and resting behavioral periods (Fig. 2). We found a significant increase in low
166 gamma power following CNO administration during running for all doses tested
167 (N=8; $F(1.904, 13.33)=9.457$, $p=0.0030$, repeated-measures one-way ANOVA with Geisser-
168 Greenhouse correction for unequal variance; 0.5 mg/kg: $p=0.0286$; 1 mg/kg: $p=0.0286$; 2 mg/kg:
169 $p=0.0286$; 4 mg/kg: $p=0.0191$, Holm-Sidak *post hoc* test for multiple comparisons versus vehicle;
170 Fig 2Biv). We also measured theta phase, low gamma amplitude coupling via
171 modulation index from hippocampal recordings during periods of running, but we
172 found no significant change in the modulation index across treatments (N=8,
173 $F(2.312, 16.19)=2.376$, $p=0.1188$, repeated-measures one-way ANOVA with Geisser-
174 Greenhouse correction for unequal variance; data not shown). During periods of rest, we
175 also found a significant increase in low gamma power following CNO
176 administration ($F(2.306, 16.15)=32.2$, $p<0.0001$, repeated-measures one-way ANOVA with
177 Geisser-Greenhouse correction for unequal variance; 0.5 mg/kg: $p=0.1008$; 1 mg/kg: $p=0.0161$; 2
178 mg/kg: $p=0.0002$; 4 mg/kg: $p=0.0004$, Holm-Sidak *post hoc* test for multiple comparisons versus
179 vehicle; Fig 2Civ). During periods of rest, beta power was significantly decreased
180 following CNO treatment compared with vehicle ($F(1.408, 9.857)=10.07$, $p=0.0066$;
181 repeated-measures one-way ANOVA with Geisser-Greenhouse correction for unequal variance;
182 0.5 mg/kg: $p=0.0486$; 1 mg/kg: $p=0.1240$; 2 mg/kg: $p=0.0545$; 4 mg/kg: $p=0.0133$, Holm-Sidak
183 *post hoc* test for multiple comparisons versus vehicle; Fig 2Ciii). High gamma power was

184 not significantly changed by CNO treatment compared with vehicle during either
185 run ($F(1.384, 9.69)=2.288$, $p=0.1602$, repeated-measures one-way ANOVA with Geisser-
186 Greenhouse correction for unequal variance, Fig 2Bv) or rest ($F(1.286, 9.003)=4.775$,
187 $p<0.0501$, repeated-measures one-way ANOVA with Geisser-Greenhouse correction for unequal
188 variance, Fig. 2Cv). In contrast, in control *Amigo2-icreERT2-* mice, during periods
189 of running, CNO treatment had no effect on low or high gamma power ($N=4$; low
190 gamma: $F(1.669, 5.006)=1.36$, $p=0.3281$; high gamma: $F(1.895, 5.684)=0.5079$, $p=0.6175$,
191 repeated-measures one-way ANOVA with Geisser-Greenhouse correction for unequal variance;
192 Fig 2D, Fig. S6).

193
194 Given the role of the hippocampal-prefrontal cortical pathway in spatial working
195 memory and the involvement of gamma synchrony between the two structures²⁹
196 as well as the previous finding that gamma synchrony is impaired in a mouse
197 model of schizophrenia²⁴, we wondered what contribution CA2 activity makes
198 toward PFC gamma oscillations. Therefore, we asked whether hippocampal low
199 gamma oscillations resulting from CA2 activation could be detected in PFC (Fig.
200 3). Using dual recordings from hippocampus and PFC, with implanted wire
201 electrodes targeting prelimbic cortex (see Fig. S4), we found that CNO treatment
202 induced significant increases in low gamma power in PFC during both run and
203 rest periods ($N=4$; run: $F(1.168, 3.505)=9.149$, $p=0.0450$; rest: $(1.561, 4.684)=4.684$,
204 $p=0.0409$, repeated-measures one-way ANOVA with Geisser-Greenhouse correction for unequal
205 variance, Fig. 3B-C). Theta, beta and high gamma powers were not affected by
206 CNO treatment (data not shown). Control *Amigo2-icreERT2-* animals showed no
207 significant change in PFC low gamma power following CNO administration ($N=4$;
208 run: $F(1.349, 4.047)=1.809$, $p=0.2617$; Fig. 3D and Fig. S7). Further, we detected no
209 significant changes in low gamma power in *Amigo2-icreERT2+* animals
210 implanted with wire electrodes that missed their PFC target ($N=3$; run: $F(1.742,$
211 $3.483)=0.7609$, $p=0.5145$; repeated-measures one-way ANOVA with Geisser-Greenhouse
212 correction for unequal variance; Fig. 3E, Fig. S4C; Fig. S8) despite those animals
213 showing increased low gamma power in hippocampus ($N=3$; $F(1.39, 2.781)=81.51$,
214 $p=0.0036$; repeated-measures one-way ANOVA with Geisser-Greenhouse correction for unequal
215 variance). These findings indicate that the increase in gamma power we detected
216 in PFC was not due to electrical artifact or brain-wide changes in activity but
217 rather to specific hippocampal inputs into the PFC^{30,31}.

218
219 Because we found increased low gamma power upon CNO administration in
220 both hippocampus and PFC, we analyzed LFP coherence between the two
221 signals to measure the extent to which the two brain areas oscillated together.
222 CNO administration produced a significant increase in low gamma coherence
223 between hippocampus and PFC during both run ($N=4$; $F(1.595, 4.786)=8.279$,
224 $p=0.0305$; repeated-measures one-way ANOVA with Geisser-Greenhouse correction for unequal
225 variance; results of Holm-Sidak *post hoc* tests versus vehicle: 0.5 mg/kg: $p=0.5808$, 1 mg/kg:
226 $p=0.2079$, 2 mg/kg: $p=0.0292$, 4 mg/kg: $p=0.0292$; Fig. 3F), and rest ($F(4, 12)=11.71$,
227 $p=0.0004$; repeated measured one-way ANOVA; results of Holm-Sidak *post hoc* tests versus
228 vehicle: 0.5 mg/kg: $p=0.1189$, 1 mg/kg: $p=0.1018$, 2 mg/kg: $p=0.0006$, 4 mg/kg: $p=0.0006$; Fig.
229 3G). In contrast, treatment with CNO produced no significant change in
230 coherence between hippocampus and PFC in control *Amigo2-icreERT2-* animals
231 ($N=4$; $F(4, 12)=1.053$, $p=0.4209$; repeated-measures one-way ANOVA; Fig. 3H).

232

233 **Increasing CA2 pyramidal cell activity decreases sharp-wave ripple**
234 **oscillations**

235 CA2 neuronal activity was recently reported to ramp up before the onset of
236 sharp-wave ripples⁷, so we were interested in whether and how modifying CA2
237 neuronal activity would impact sharp-wave ripples recorded in CA1. Therefore,
238 we measured ripple oscillations from the CA1 pyramidal cell layer of *Amigo2-*
239 *icreERT2+* and control *Amigo2-**icreERT2-* mice infused with hM3Dq during
240 periods of rest 30-60 minutes following administration of either CNO (0.5 mg/kg,
241 SQ; Fig. 4) or vehicle as control. We chose to use a low dose of CNO in this
242 experiment to minimize the possibility that ripple-filtered LFPs would be
243 contaminated by neuronal spiking in response to CNO administration
244 independent of ripple-associated spiking. In *Amigo2-**icreERT2+* animals, CNO
245 administration significantly decreased ripple event rate relative to that observed
246 following vehicle administration (N=8; $t(7)=4.574$, $p=0.0026$; two-tailed paired t-test; Fig.
247 4C), although ripple amplitude was not significantly affected ($t(7)=0.3004$, $p=0.7726$;
248 two-tailed paired t-test; Fig. 4D). In control *Amigo2-**icreERT2-* animals, CNO
249 administration had no effect on ripple event rate or amplitude (N=4; event rate:
250 $t(3)=1.871$, $p=0.1581$; amplitude: $t(3)=0.3193$, $p=0.7704$; two-tailed paired t-test; Fig. 4E-F).
251 Further experiments in a different line of hM3Dq-expressing animals are
252 presented in Fig. S13-S17.

253

254 **CA2 pyramidal cell inhibition decreases hippocampal and prefrontal**
255 **cortical low gamma power.**

256 Based on our finding that increasing activity of CA2 neurons in hM3Dq-
257 expressing mice increased low gamma power in hippocampus and PFC, we
258 hypothesized that inhibition of CA2 pyramidal neurons with hM4Di would
259 decrease gamma power. As a control experiment to ascertain whether hM4Di
260 would decrease CA2 synaptic output in our system, we infused *Amigo2-*
261 *icreERT2+* mice with AAV-EF1a-DIO-hChR2(H134R)-EYFP (ChR2) and hM4Di
262 AAVs, treated animals with tamoxifen, and then implanted the animals with fiber
263 optic probes in CA2 and electrode bundles in the ipsilateral intermediate CA1.
264 Optogenetic stimulation of CA2 in these awake, behaving animals evoked
265 detectable voltage responses in CA1 that were inhibited as early as 20 min post
266 CNO treatment (the earliest we tested). In this preparation, we detected inhibition
267 of CA2 responses for 4 hours. By 24 hours, responses recovered to 77.20% of
268 pre-CNO response amplitude (Fig. S9).

269

270 To test our hypothesis that hM4Di inhibition of CA2 output would decrease
271 hippocampal and prefrontal cortical low gamma power, we recorded LFPs from
272 *Amigo2-**icreERT2+* and control *Amigo2-**icreERT2-* mice infused with hM4Di AAV,
273 treated with tamoxifen and implanted with electrodes. Hippocampal LFPs were
274 measured from the primary target of CA2 pyramidal neurons, CA1 (4 mice with
275 dorsal CA1 electrodes, 4 mice with intermediate CA1 electrodes, Fig. S10),
276 because the majority of the neuronal inhibition by hM4Di occurs at the axon
277 terminal to reduce neurotransmitter release³². Using identical analyses as for

278 hM3Dq-infused animals, we compared LFPs filtered in the theta (5-10 Hz), beta
279 (14-18 Hz), low gamma (30-60 Hz) and high gamma (65-100 Hz) frequency
280 ranges during periods of running and resting 30-60 minutes following
281 administration of CNO (5 mg/kg, SQ) or vehicle. We found a significant decrease
282 in low gamma power during running following CNO administration compared with
283 vehicle ($t(7)=4.408$, $p=0.0031$, two-tailed paired t-test, Fig. 5Aiv, Fig. 5F). However,
284 modulation index, a measure of theta phase, gamma amplitude coupling, was not
285 significantly affected by CNO administration during running ($t(7)=2.07$, $p=0.0772$; two-
286 tailed paired t-test, data not shown). We also found a significant increase in beta power
287 during running following CNO administration compared with vehicle ($t(7)=2.401$,
288 $p=0.0474$, two-tailed paired t-test, Fig. 5Aiii). Treatment with CNO did not affect theta
289 or high gamma power during running and did not affect power in any of these
290 frequency bands during periods of rest (Fig. 5A-B).

291
292 CA2 pyramidal neurons have been shown to possess axons with large rostral to
293 caudal trajectories, primarily targeting CA1³³. Consistent with a projection toward
294 caudal CA1, we observed fluorescence from hM4Di-mCherry+ axon fibers in
295 caudal intermediate CA1, with most of the fluorescently-labeled CA2 axons
296 targeting *stratum oriens* in CA1²⁸ (Fig. 5C). CA1 neurons, in turn, project to
297 PFC^{31,34,35}. Therefore, we asked whether inhibition of CA2 pyramidal neurons
298 would impact low gamma power recorded in PFC. A subset of *Amigo2*-
299 *icreERT2*+ and control *Amigo2*-*icreERT2*- mice with electrodes in CA1 were also
300 implanted with electrodes in PFC and treated with CNO (5 mg/kg, SQ) or vehicle
301 control. In *Amigo2*-*icreERT2*+ mice, we observed a significant decrease in PFC
302 low gamma power during running following CNO administration compared with
303 vehicle ($N=6$; $t(5)=2.948$, $p=0.0320$; two-tailed paired t-test; Fig. 5D), suggesting that CA2
304 activity modulates PFC low gamma oscillations, likely via intermediate CA1.
305 Control *Amigo2*-*icreERT2*- animals showed no significant change in hippocampal
306 or PFC low gamma power in response to CNO treatment compared with vehicle
307 ($N=5$; hippocampus: $t(4)=1.079$, $p=0.3413$, two-tailed paired t-test; PFC: $t(4)=0.4293$, $p=0.6898$,
308 two-tailed paired t-test; Fig. 5E).

309 CA2 pyramidal cell inhibition increases hippocampal ripple oscillations.

310 To assess the influence of inhibiting CA2 output on ripple oscillations, we
311 measured ripples from the CA1 pyramidal cell layer in *Amigo2*-*icreERT2*+ and
312 control *Amigo2*-*icreERT2*- mice during periods of rest, 30-60 minutes following
313 administration of either CNO (5 mg/kg, SQ) or vehicle control. As predicted
314 based on our findings in hM3Dq-infused animals, CNO administration
315 significantly increased ripple event rate in hM4Di-infused animals ($N=6$; $t(5)=3.809$,
316 $p=0.0063$; one-tailed paired t-test; Fig. 6C). CNO administration also increased ripple
317 amplitude in hM4Di animals ($t(5)=3.069$, $p=0.0278$; two-tailed paired t-test; Fig. 6D). By
318 contrast, in control *Amigo2*-*icreERT2*- mice, CNO administration did not
319 significantly change ripple event rate or amplitude ($N=6$; event rate: $W=5$, $p=0.6875$,
320 Wilcoxon signed-ranked test; amplitude: $t(5)=0.5165$, $p=0.6275$, two-tailed paired t-test; Fig. 6E-
321 F). These data, together with our hM3Dq ripple findings, indicate that
322

323 hippocampal ripple occurrence is negatively modulated by activity of CA2
324 pyramidal neurons.

325

326 **CA2 pyramidal cell inhibition decreases social preference.**

327 To determine whether oscillatory effects of silencing CA2 correlate with specific
328 behavioral effects, we tested hM4Di-infused *Amigo2-icreERT2+* and control
329 *Amigo2-icreERT2-* mice in behavioral assays following CNO administration.
330 Based on our findings of reduced low gamma power in hippocampus and PFC in
331 hM4Di animals, and because previous findings report reduced low gamma
332 coherence between hippocampus and PFC²⁴ as well as increased sharp-wave
333 ripple occurrence³⁶ in animal models of schizophrenia, we focused on behaviors
334 shown to be impaired in animal models of schizophrenia, including social
335 behavior, prepulse inhibition and spatial working memory³⁷.

336

337 Social behavior was assessed in male and female *Amigo2-icreERT2+* and
338 control *Amigo2-icreERT2-* mice infused with hM4Di AAV using the social
339 approach assay following administration of CNO (5 mg/kg, IP; Fig. 7). CNO-
340 treated control *Amigo2-icreERT2-* mice favored the social chamber over the
341 empty chamber. However, *Amigo2-icreERT2+* animals showed no significant
342 preference for the social chamber upon CNO administration (male and female mice
343 combined: main effect of chamber: $F(1,22)=9.852$, $p=0.0048$; main effect of genotype:
344 $F(1,22)=0.06729$, $p=0.7977$, repeated measures two-way ANOVA; time spent in social versus
345 empty chamber: Cre+: $F(1, 11)=1.15$; $p=0.3057$; Cre-: $F(1, 11)=13.52$; $p=0.0037$, within-genotype
346 repeated measures ANOVA; Fig. 7B, Fig. S11). Further, although our experiments
347 were not powered to detect differences due to sex, a sex-specific difference
348 emerged: the effect of CA2 inhibition on social approach appeared to be driven
349 exclusively by the male animals (Fig. 7C). Among females, *Amigo2-icreERT2+*
350 mice showed similar preference for the social chamber over the empty chamber
351 as *Amigo2-icreERT2-* mice (N=8; main effect of chamber: $F(1, 6)=106.6$, $p<0.0001$; main
352 effect of genotype: $F(1, 6)=0.001545$, $p=0.9699$, repeated measures two-way ANOVA; time spent
353 in social chamber versus empty chamber: Cre+: $p=0.0005$; Cre-: $p=0.0002$, within-genotype
354 repeated measures ANOVA). By contrast, among males, *Amigo2-icreERT2+* mice did
355 not show a preference for the social chamber, while *Amigo2-icreERT2-* mice did
356 (N=16; main effect of chamber: $F(1, 14)=3.123$, $p=0.0990$; main effect of genotype: $F(1,$
357 $14)=0.08210$, $p=0.7787$, repeated measures two-way ANOVA; time spent in social chamber
358 versus empty chamber: Cre+: $p=0.7932$; Cre-: $p=0.0425$, within-genotype repeated measures
359 ANOVA).

360

361 Prepulse inhibition of acoustic stimuli and spatial working memory were also
362 assessed in hM4Di-infused *Amigo2-icreERT2+* and *Amigo2-icreERT2-* mice
363 administered CNO (5 mg/kg, IP; Fig. S12). We failed to detect any significant
364 differences between *Amigo2-icreERT2+* and *Amigo2-icreERT2-* mice in any of
365 the prepulse inhibition measures (Fig. S12A-C). To assess spatial working
366 memory, the number and percent of spontaneous alternations were measured
367 while animals explored a Y-maze. Again, we found no differences between
368 *Amigo2-icreERT2+* and *Amigo2-icreERT2-* mice in this measure of working
369 memory (Fig. S12D-F).

370

371 **DISCUSSION**

372 In this study, we used excitatory and inhibitory DREADDs to reversibly modify
373 activity of CA2 pyramidal cells and examined the effect on hippocampal and
374 prefrontal cortical oscillations and behavior. We found that increasing activity of
375 CA2 pyramidal cells increased hippocampal and prefrontal cortical low gamma
376 power and decreased hippocampal sharp-wave ripples. Conversely, we found
377 that inhibiting CA2 pyramidal cell output decreased hippocampal and prefrontal
378 cortical low gamma power and increased hippocampal sharp-wave ripples.
379 Behaviorally, inhibiting CA2 output decreased social approach behavior. These
380 findings demonstrate a role for hippocampal area CA2 in low gamma oscillation
381 generation across the distributed hippocampal-prefrontal cortical network.
382 Further, these findings support a negative regulatory role of CA2 in hippocampal
383 sharp-wave ripples and provide further support for the role of CA2 in social
384 behavior.

385
386 CA2 activation produced robust, dose-dependent increases in hippocampal low
387 gamma power, and inhibition of CA2 neurons decreased low gamma power.
388 Gamma oscillations in hippocampus reflect synchronous inhibitory postsynaptic
389 potentials (IPSPs) from a network of interconnected perisomatically-targeted
390 basket cells, with excitatory drive onto these interneurons arising from pyramidal
391 cells³⁸⁻⁴⁰. The frequency of the gamma oscillations is controlled by the decay
392 kinetics of the IPSP such that slower decay yields a lower gamma frequency³⁹.
393 Low gamma oscillations in CA1 reportedly arise from neuronal activity in CA3^{9,11}.
394 However, permanent silencing of CA3 output with tetanus toxin light chain
395 produced only a 30% reduction in low gamma power recorded in CA1¹⁷, thereby
396 challenging the notion that CA3 is the only origin of hippocampal low gamma
397 oscillations. Here, we report that CA2 activation increases low gamma power and
398 that acute CA2 silencing reduces low gamma power recorded in CA1 by
399 approximately 20%. Although tetanus toxin light chain abolishes neurotransmitter
400 release, hM4Di is reported to substantially, but not entirely, inhibit synaptic
401 neurotransmitter release³² (see also Fig. S9). As such, complete silencing of CA2
402 would likely reduce low gamma power by greater than the 20% we observed
403 here. Based on these findings, CA2 and CA3 together likely provide the
404 excitatory drive required to generate low gamma oscillations in CA1. Given the
405 dynamic nature of the brain, we propose that when CA2 is inhibited, CA3, or
406 another source, is capable of compensating, and vice versa. Further, gamma
407 activity arising from CA2 and CA3 may engage distinct circuits involving the deep
408 and superficial CA1 pyramidal neurons, respectively^{28,41}. As such, gamma
409 oscillations arising from the two areas may subserve distinct cognitive functions
410 based on the output of these two populations.

411
412 Modification of CA2 neuronal activity also affected the occurrence of sharp-wave
413 ripple oscillations. Specifically, increasing CA2 activity with hM3Dq decreased
414 the occurrence of ripples, whereas decreasing CA2 output with hM4Di increased
415 ripple occurrence as well as amplitude. The mechanism underlying these findings

416 likely includes the robust inhibition that CA2 presents over CA3 neurons^{8,28}.
417 Accordingly, CA2 pyramidal cells contact local parvalbumin-expressing basket
418 cells, which project to CA3⁴², and CA2 pyramidal cell firing is reported to
419 discharge CA3 interneurons⁷. As a potential secondary mechanism underlying
420 the observed inverse relationship between CA2 neuronal activity and occurrence
421 of ripples, CA2 neurons preferentially target the deep layer of pyramidal cells in
422 CA1²⁸. During recordings of ripples from these deep CA1 pyramidal cells,
423 dominant hyperpolarizations are observed, which contrasts with dominant
424 depolarizations during ripples seen in superficial CA1 pyramidal cells⁴³ (see
425 also⁴¹). Further, stimulation of CA2 neurons produces robust feed-forward
426 inhibitory responses onto CA1 neurons^{8,43}. Therefore, silencing of CA2 neurons
427 may remove feed-forward inhibition and produce a net excitatory response in
428 CA1. Together, these two mechanisms may explain the significant gating
429 influence that CA2 neurons have over hippocampal excitability and,
430 consequently, sharp-wave ripples in CA1.

431
432 Consistent with this finding, mice in which CA2 synaptic output was fully and
433 permanently blocked via tetanus toxin light chain showed normal ripples during
434 immobility and also anomalous epileptiform discharges that arose from CA3⁸.
435 Our findings of increased ripples in CA1 upon acute silencing of CA2 output are
436 consistent with these findings in that in both studies, CA2 silencing increases
437 CA3 to CA1 output during immobility. Echoing the statement by Boehringer et al⁸,
438 our data do not agree with the suggestion by Oliva et al.⁷ that CA2 neuronal
439 activity triggers the occurrence of ripples. Rather, CA2 activity may play a role in
440 sculpting the CA3 network activity and gate output to CA1. Consistent with a
441 gating, or permissive, role of CA2 toward the occurrence of ripples, Kay et al.
442 revealed that CA2 is the only hippocampal subregion to have a substantial
443 population of neurons that cease firing during CA1 ripples⁶. Similarly, Oliva et al.
444 demonstrated an inverse correlation between occurrence of ripples in CA2 and
445 CA1. During periods of low occurrence of ripples in CA2, ripple occurrence was
446 high in CA1, and vice versa⁷. The inverse correlations described by these two
447 findings suggest a negative regulatory role of CA2 activity on CA1 ripples, which
448 is consistent with our findings.

449
450 Our findings also reveal a role for CA2 in beta oscillations in that CA2 activation
451 decreased beta power whereas CA2 inhibition increased beta power. Although
452 these oscillations have been studied far less than gamma and ripple oscillations,
453 they are thought to contribute to hippocampal novelty detection processes; beta
454 power is increased on exposure to a novel environment and decreases with
455 repeated exposure^{44,45}. A role for CA2 in oscillations that reflect novelty detection
456 seems fitting given our recent findings that CA2 place fields are remapped upon
457 exposure to novel environmental stimuli² and other studies demonstrating CA2
458 responsiveness to novelty^{5,46}.

459
460 We and others have demonstrated a significant role for CA2 in social behavior.
461 Using mice with CA2 chronically silenced with tetanus toxin light chain, Hitti and

462 Siegelbaum presented evidence that CA2 activity is required for one form of
463 social recognition memory²⁰. In addition, we recently demonstrated that CA2
464 neuron spatial representations (place fields) remap upon exposure to novel or
465 familiar conspecific animals². These effects may involve vasopressinergic
466 signaling because deletion of one of the vasopressin receptors (*Avpr1b*) that
467 shows selective expression in CA2 results in impaired social behavior, including
468 aggression²¹, and optogenetic stimulation of vasopressin-containing axon fibers
469 in CA2 enhances social memory²². Interestingly, both vasopressin and oxytocin
470 receptor agonists enhance Schaffer Collateral synaptic transmission in CA2²¹.
471 Here, we report that acute inhibition of CA2 neurons with hM4Di impairs social
472 approach behavior. Remarkably, the social approach impairment we observed
473 may be specific to male mice in that our female, but not male, hM4Di mice
474 behaved similar to controls. Of note, previous studies of CA2 and social behavior
475 used only male rodents^{2,20-22,47}. The mechanism underlying this dimorphic effect
476 may include vasopressin and/or oxytocin, but whether axon fibers containing
477 these molecules differentially innervate CA2 in males and females, or whether
478 Schaffer Collateral synaptic potentiation²¹ or other effects induced by these
479 peptides differ by sex is unknown. Indeed, though, sex differences in dendritic
480 branching patterns of CA2 neurons have been reported in guinea pig⁴⁸, so it
481 stands to reason that other sex differences may exist in CA2.

482
483 The results of our study present further similarities between CA2 functions and
484 impairments seen in schizophrenia. Gamma oscillations and social behavior are
485 both impaired in patients with schizophrenia^{49,50}. In addition, parvalbumin-
486 expressing interneurons, which contribute to the generation of gamma
487 oscillations, are notably lost from hippocampal area CA2 and PFC in tissue from
488 patients with this disorder^{51,52}. Findings from the *Df16A*^{+/-} mouse model of
489 schizophrenia demonstrate impaired social behavior, decreased number of
490 parvalbumin-expressing interneurons in CA2, decreased activity of CA2
491 pyramidal neurons²³, and decreased synchrony between hippocampus and
492 PFC²⁴. Additionally, the forebrain-selective calcineurin knock-out model of
493 schizophrenia was reported to have increased CA1 ripple events during periods
494 of resting wake³⁶. We report that CA2 neuronal activity contributes to low gamma
495 oscillations in both hippocampus and PFC, gamma coherence between
496 hippocampus and PFC, hippocampal ripple oscillations and to social behavior,
497 suggesting that CA2 may play a role in the pathophysiology of schizophrenia, or
498 possibly the social deficits therein.

499
500 Here, we have provided evidence that CA2 neuronal activity bidirectionally
501 controls hippocampal and prefrontal cortical low gamma oscillations as well as
502 hippocampal beta and sharp-wave ripple oscillations. Further, we provide
503 evidence that CA2 activity is required for social approach behavior, but perhaps
504 only in male mice. These findings demonstrate a role for CA2 in the extended
505 hippocampal-prefrontal cortical network and further support the idea that CA2 is
506 an integral node in the hippocampal network relating to social cognition.

507

508 **Online Methods:**

509 **Animals**

510 Experiments were carried out in adult male and female mice (8–12 weeks at the
511 start of experiments). Mice were housed under a 12:12 light/dark cycle with
512 access to food and water *ad libitum*. Mice were naïve to any treatment,
513 procedure or testing at the time of beginning the experiments described here.
514 Mice were group-housed until the time of electrode implantation for those mice
515 undergoing electrode implantation surgery, at which point they were singly
516 housed. All procedures were approved by the NIEHS Animal Care and Use
517 Committee and were in accordance with the National Institutes of Health
518 guidelines for care and use of animals.

519

520 **Generation of transgenic *Amigo2*-icreERT2**

521 The BAC clone RP23-288P18 was used to generate these mice. To recombine
522 the cDNA encoding an icreERT2 fusion protein⁵³ into the BAC, we constructed a
523 targeting vector from which we derived a targeting fragment for recombineering.
524 The targeting fragment consisted of a 243 bp homology region (A-Box)
525 immediately upstream of the ATG in the *Amigo2* gene. The icreERT2 cassette
526 was fused to the A-Box replacing the *Amigo2* ATG with the icre ATG preceded
527 with a perfect KOZAK sequence. At the 3' end of the icreERT2 cassette a
528 synthetic bovine growth hormone (BGH) polyadenylation signal was added after
529 the STOP codon. For selection of recombined BACs, a flipase-site flanked
530 neomycin resistance gene was incorporated into the targeting fragment following
531 the icreERT2 cassette. Finally, the 3' end of the targeting fragment contained a
532 263 bp homology region (B-Box) starting downstream of the *Amigo2* ATG.
533 Recombineering was performed according to a previously described protocol⁵⁴.
534 In brief, the targeting fragment was electroporated into induced EL250 bacteria
535 harboring the *Amigo2* BAC. Recombined colonies were selected on
536 Chloramphenicol/Kanamycin plates and screened by colony PCR. The neo gene
537 was removed from the recombined BAC by arabinose driven flipase expression.

538

539 Recombined BACs without the neo marker were linearized by restriction enzyme
540 digestion, gel purified and electro-eluted from the gel slice. After filter dialysis
541 with a Millipore VSWP02500 filter, the BAC fragment concentration was adjusted
542 to 1 ng/μl and microinjected into pronuclei of B6SJLF1 mouse oocytes (Taconic,
543 North America). Six independent founder mice resulted, which were bred to
544 *ROSA*-tdTomato indicator mice. Resulting offspring that genotyped positive for
545 both Cre and tdTomato were treated with tamoxifen (Sigma, 100 mg/kg daily
546 administration, IP, 7 days of treatment). At least one week following the final
547 treatment with tamoxifen, mice were perfused with 4% paraformaldehyde and
548 brains were sectioned and examined for tdTomato expression. Two lines showed
549 adult expression of icreERT2 in CA2; one showed sparse expression in dentate
550 gyrus and was not used in this study, another (line 1; *B6(SJL)-Tg(Amigo2-
551 icre/ERT2)1Ehs*) showed selective expression in CA2 within hippocampus as
552 well as expression in fasciola cinerea and hypothalamus, among other locations

553 (Supplementary Figure 1). Line 1 mice were used for electrophysiology, anatomy
554 and behavioral studies here and were bred to *ROSA*-tdTomato (described
555 above), *GAD*-eGFP, or *GAD*-eGFP; *ROSA*-tdTomato mice for histological
556 analysis. *Amigo2*-*icreERT2* mice used in this study were backcrossed to C57Bl/6
557 7 generations.

558

559 Genotyping of *Amigo2*-*icreERT2* BAC transgenic mice was done using the
560 following primers: BGH-F (forward primer) 5'-CTT CTG AGG CGG AAA GAA
561 CC-3' and dAmigo4 (reverse primer) 5'-AACTGCCCGTGGAGATGCTGG-3'.
562 PCR protocol is 30 cycles of 94°C 30 sec., 60°C 30 sec., 72°C 30sec. PCR
563 product is 600bp.

564

565 Animal Numbers

566 For all experiments presented, 89 *Amigo2*-*icreERT2* mice (8 for histology, 50 for
567 behavior, 29 for electrophysiology, 2 for optogenetics with electrophysiology), 13
568 *Amigo2*-*icreERT2*; *ROSA*-tdTomato mice (all for histology), 3 *Amigo2*-*icreERT2*;
569 *GAD*-eGFP; *ROSA*-tdTomato mice (all for histology) and 4 *Amigo2*-*icreERT2*;
570 *GAD*-eGFP mice (all for histology) were used. No statistical tests were used to
571 determine sample sizes *a priori*, but sample sizes for histological,
572 electrophysiological and behavioral studies were similar to those used in the
573 field. For electrophysiology studies, *Amigo2*-*icreERT2*⁺ and *Amigo2*-*icreERT2*⁻
574 animals were randomly selected from litters. For behavioral studies, pairs of
575 *Amigo2*-*icreERT2*⁺ and *Amigo2*-*icreERT2*⁻ animals were randomly selected from
576 individual litters and infused with DREADD AAVs. For randomization, animals
577 were housed with same-sex littermates following weaning but before genotyping.
578 Genotype information was unknown at the time of randomly selecting a mouse
579 from the cage for AAV infusion.

580

581 Virus infusion and tamoxifen treatment

582 Viruses were obtained from the viral vector core at the University of North
583 Carolina-Chapel Hill. Mice were infused with AAV-hSyn-DIO-hM3D(Gq)-mCherry
584 (Serotype 5; hM3Dq AAV), AAV-hSyn-DIO-hM4D(Gi)-mCherry (Serotype 5;
585 hM4Di AAV) or equal parts AAV-EF1a-DIO-hChr2(H134R)-EYFP (Serotype 5;
586 Chr2 AAV) and hM4Di mixed in a centrifuge tube. For virus-infusion surgery,
587 mice were anesthetized with ketamine (100 mg/kg, IP) and xylazine (7 mg/kg,
588 IP), then placed in a stereotaxic apparatus. An incision was made in the scalp, a
589 hole was drilled over each target region for AAV infusion, and a 27-ga cannula
590 connected to a Hamilton syringe by a length of tube was lowered into
591 hippocampus (in mm: -2.3 AP, +/-2.5 ML, -1.9 mm DV from bregma). *Amigo2*-
592 *icreERT2* mice were infused unilaterally on the left side for hM3Dq AAV infusion,
593 bilaterally for hM4Di AAV, or unilaterally on the left side for Chr2/hM4Di infusion.
594 For each infusion, 0.5 µl was infused at a rate of 0.1 µl/min. Following infusion,
595 the cannula was left in place for an additional 10 minutes before removing. The
596 scalp was then sutured and the animals administered buprenorphine (0.1 mg/kg,
597 SQ) for pain and returned to their cage. Two weeks following AAV infusion
598 surgery, *Amigo2*-*icreERT2* mice began daily tamoxifen treatments (100 mg/kg

599 tamoxifen dissolved in warmed corn oil, IP) for a total of 7 days. At least one
600 week following the last dose of tamoxifen, animals were euthanized and perfused
601 with 4% paraformaldehyde for anatomical studies, or underwent electrode (and
602 fiber optic probe for ChR2/hM4Di mice) implantation surgery, or were transferred
603 to the University of North Carolina Mouse Behavioral Phenotyping Laboratory in
604 Chapel Hill, NC. At least three weeks was allowed to elapse between the last
605 dose of tamoxifen and the beginning of the behavioral studies.

606

607 Electrode Implantation

608 At least one week after the last tamoxifen treatment, mice for *in vivo*
609 electrophysiology were implanted with electrode arrays. Mice were anesthetized
610 with ketamine (100 mg/kg, IP) and xylazine (7 mg/kg, IP), then placed in a
611 stereotaxic apparatus. An incision was made in the scalp, and the skull was
612 cleaned and dried. One ground screw (positioned approximately 4 mm posterior
613 and 2 mm lateral to Bregma over the right hemisphere) and four anchors were
614 secured to the skull and electrode arrays were then lowered into drilled holes
615 over the target brain regions. Electrode wires were connected to a printed circuit
616 board (San Francisco Circuits, San Mateo, CA), which was connected to a
617 miniature connector (Omnetics Connector Corporation, Minneapolis, MN). For all
618 but one mouse that was implanted with tetrodes, electrodes consisted of
619 stainless steel wire (44- μ m) with polyimide coating (Sandvik Group, Stockholm,
620 Sweden). Wires were bundled into groups of 8 and lowered to target regions. In
621 11 *Amigo2-icreERT2* mice infused with hM3Dq AAV (7 Cre+, 4 Cre-) and 8
622 *Amigo2-icreERT2* mice infused to hM4Di AAV (2 Cre+, 6 Cre-), electrode arrays
623 were implanted into the left dorsal hippocampus, targeting CA2/proximal CA1 (in
624 mm: -2.06 AP, -2.5 ML, -1.9 DV from bregma), the right dorsal hippocampus
625 targeting CA1 (-1.94 AP, +1.5 ML, -1.5 DV from bregma), and the left PFC (+1.78
626 AP, -0.25 ML, -2.35 DV from bregma). In 4 *Amigo2-icreERT2* mice infused with
627 hM4Di AAV (4 Cre+), electrodes were lowered into left dorsal hippocampus
628 targeting CA2/proximal CA1 (-2.06 AP, -2.5 ML, -1.9 DV from bregma), left PFC
629 (+1.78 AP, -0.25 ML, -2.35 DV from bregma) and left intermediate hippocampus
630 targeting CA1 (-2.92 AP, 2.75 ML, 2.1 DV from bregma). In 3 *Amigo2-icreERT2*
631 mice infused with hM3Dq AAV (3 Cre+), electrodes were implanted in left dorsal
632 hippocampus targeting CA2/proximal CA1 only (-2.06 AP, -2.5 ML, -1.9 DV from
633 bregma). In 2 *Amigo2-icreERT2* mice infused with hM4Di AAV (2 Cre+),
634 electrodes were implanted in left hippocampus targeting CA1 only (-1.94 AP,
635 +1.5 ML, -1.25 DV from bregma). In one *Amigo2-icreERT2+* infused with hM3Dq
636 AAV, a bundle of 8 tetrodes was lowered into the left hippocampus targeting
637 CA2/proximal CA1 (-2.06 AP, -2.5 ML, -1.9 DV from bregma) for monitoring
638 changes in single unit firing rate upon CNO administration. In 2 *Amigo2-*
639 *icreERT2+* mice infused with ChR2/hM4Di AAV, a fiber optic probe was
640 implanted into left CA2 (-1.95 AP, -2.25 ML, -1.65 DV from bregma) and a wire
641 bundle was implanted into left intermediate CA1 (-3.08 AP, -2.75 ML, -2.0 DV
642 from bregma).

643

644 Histology

645 Animals used for histology were euthanized with Fatal Plus (sodium
646 pentobarbital, 50 mg/mL; >100 mg/kg) and underwent transcordial perfusion with
647 4% paraformaldehyde. Brains were then cryoprotected in 30% sucrose PBS for
648 at least 72 hours and sectioned with a cryostat or vibratome at 40 μ m.

649
650 For immunohistochemistry, brain sections were rinsed in PBS, boiled in
651 deionized water for 3 min, and blocked for at least 1 h in 3-5% normal goat
652 serum/0.01% Tween 20 PBS. Sections were incubated in the following primary
653 antibodies, which have previously been validated in mouse brain^{20,28}: rabbit anti-
654 PCP4 (SCBT, sc-74186, 1:500), rabbit anti-CaMKII alpha (Abcam, ab131468,
655 1:250), rat anti-mCherry (Life Technologies, M11217, 1:500- 1:1000), mouse
656 anti-cre (Millipore, 3120, 1:5000), mouse anti-calbindin (Swant, D-28k, 1:500).
657 Antibodies were diluted in blocking solution and sections were incubated for 24 h.
658 After several rinses in PBS/Tween, sections were incubated in secondary
659 antibodies (Alexa goat anti-mouse 488 and Alexa goat anti-rabbit 568, Alexa
660 Goat anti-rat 568, Invitrogen, 1:500) for 2 h. Finally, sections were washed in
661 PBS/Tween and mounted under ProLong Gold Antifade fluorescence media with
662 DAPI (Invitrogen). Images of whole-brain sections were acquired with a slide
663 scanner using the Aperio Scanscope FL Scanner, (Leica Biosystems Inc.). The
664 slide scanner uses a monochrome TDI line-scan camera, with a PC-controlled
665 mercury light source to capture high resolution, seamless digital fluorescent
666 images. Images of hippocampi were acquired on a Zeiss 780 meta confocal
667 microscope using a 40 \times oil-immersion lens. Counts were made of cells
668 expressing the Cre-dependent tdTomato fluorescent reporter. Five *Amigo2-*
669 *icreERT2+; ROSA-tdTomato +/-* mice were used for this analysis with 3-5 50- μ m
670 sections per animal spanning the anterior-posterior extent of CA2. Sections were
671 stained for PCP4 and colocalization of PCP4 with tdTomato was assessed in a
672 total of 5,248 cells.

673
674 Neurophysiological data acquisition and behavioral tracking
675 Neural activity was transmitted via a 32-channel wireless 10 \times gain headstage
676 (Triangle BioSystems International, Durham, NC) and was acquired using the
677 Cerebus acquisition system (Blackrock Microsystems, Salt Lake City, UT).
678 Continuous LFP data were band-pass filtered at 0.3–500 Hz and stored at
679 1,000 Hz. Single unit data were sampled at 30 kHz and high-pass filtered at
680 250 Hz. Neurophysiological recordings were referenced to a silver wire
681 connected to a ground screw secured in the posterior parietal bone. To confirm
682 that gamma power activity recorded in hippocampus and PFC were not artifacts
683 of differential recording between the active electrode and the ground screw, in
684 some animals, one wire per bundle targeting hippocampus or PFC, was
685 positioned either in the cortex above hippocampus or in the striatum lateral to
686 PFC. Referencing signals to these short or lateral wires showed LFPs that
687 increased or decreased in gamma power upon CNO administration to hM3Dq or
688 hM4Di-infused mice, respectively, similar to recordings that were referenced to
689 the ground screw. For behavioral tracking, the X and Y coordinates in space of a
690 light-emitting diode (for use with color camera) or a small piece of reflective tape

691 (for use with infrared camera) present on the wireless headstage were sampled
692 at 30 Hz using Neuromotive Software (Blackrock Microsystems) and position
693 data were stored with the neural data.

694

695 For recordings from mice infused with hM3Dq AAV, baseline data was acquired
696 for at least 20 minutes followed by treatment with vehicle (10% DMSO in saline)
697 or CNO (0.05-4 mg/kg CNO dissolved in DMSO to 50 mM then suspended in
698 saline, SQ) and recording continued for an additional 2 hours. During the entire
699 recording time, mice were inside of an open field arena, which was a custom-
700 built, 5-sided (open top) dark arena (approximately 80 cm long x 80 cm wide x
701 100 cm high). The walls and floor of the arena were constructed from black-
702 colored Plexiglass. Mice administered various doses of CNO were first treated
703 with vehicle and then increasing doses of CNO at three-day intervals. Room light
704 remained illuminated, but a curtain was placed around the open field chamber
705 during recordings. For neurophysiology experiments on hM4Di AAV-infused
706 mice, after connecting headstages to the animals' electrodes, animals were
707 administered either vehicle or CNO (5 mg/kg, SQ) then returned to their cage for
708 30 minutes before starting recording. Room lights were turned off and red lights
709 were illuminated after administering vehicle or CNO. After 30 minutes had
710 elapsed, mice were placed in the open field arena for recording. Gamma power
711 measurements were made during periods when the animals were moving at ≥ 7
712 cm/sec. Ripple measurements were made when the animals were moving ≤ 0.5
713 cm/sec.

714

715 Following recordings, neurons for single-unit recordings were sorted into
716 individual units by tetrode mode-based cluster analysis in feature space using
717 Offline Sorter software (Plexon Inc., Dallas, TX). Autocorrelation and cross-
718 correlation functions of spike times were used as separation tools. Only units with
719 clear refractory periods and well-defined cluster boundaries were included in the
720 analyses. Pyramidal cells and interneurons were distinguished based on
721 autocorrelation plots (peak within 10 msec representing bursting), waveforms
722 (broad waveforms, with a peak to valley spike width of >300 μ sec) and mean
723 firing rates (<5 Hz during baseline recording)⁵⁵. Only pyramidal cells were
724 included in analyses.

725

726 For simultaneous optogenetic stimulation and LFP recording, fiber optic probes
727 (200 μ m diameter) were connected to a Plexbright 4-channel optogenetics
728 controller through a wired tether, and Radiant software (Plexon, Inc.) was used to
729 drive light stimulation. Electrophysiological recordings were made from awake,
730 behaving mice during periods of run and rest (behavioral state not separated for
731 these experiments) using 32 channel head stages digitized at 16-bit resolution
732 and acquired at 40 kHz using the OmniPlex D Neural Data Acquisition
733 System (Plexon, Inc.). Continuous neural data were low pass filtered at 500 Hz
734 and sampled at 1000 Hz. For these experiments, baseline recordings were
735 obtained for several minutes before delivering fiber optic stimulation. Stimulation
736 consisted of 5 pulses delivered at 10 Hz, with each pulse being 5 msec in

737 duration and with a current intensity of 200 mA delivered to the light emitting
738 diode. One train was delivered per minute for 3 minutes. Animals were then
739 administered either vehicle or CNO (5 mg/kg, SQ), and LFP responses to light
740 stimulation were made following identical stimulation parameters between 20
741 minutes and 24 hours following vehicle/CNO treatment. Response amplitudes
742 were measured from evoked voltage deflections time locked to the optogenetic
743 stimulation events.

744

745

746 Electrode localization

747 Upon completion of electrophysiology studies, mice were perfused with 4%
748 paraformaldehyde. Heads with electrodes remaining in place in brains were then
749 submerged in 4% paraformaldehyde for 24-48 h. Electrodes were carefully
750 removed and brains were submerged in 30% sucrose/PBS and sectioned at
751 40 μm on a cryostat or vibratome.

752

753 Electrophysiology Data Analysis

754 The experimenter was blind to the genotype of animals at the time of data
755 analysis. All neuronal data analyses were performed using Neuroexplorer
756 software (Nex Technologies, TX) and Matlab (MathWorks, Inc., Natick, MA) with
757 the Chronux toolbox for Matlab (<http://chronux.org/>). Statistical analyses were
758 performed using GraphPad Prism version 6.

759

760 Identical analyses were used for all hM3Dq and hM4Di spectral measures. Data
761 were first divided into periods of running (>7 cm/sec) or resting (<0.5 cm/sec and
762 limited to up to 20 sec once an animal has started moving <0.5 cm/sec). These
763 LFP subsets were then z-scored to control for changes in overall signal
764 amplitude (and, consequently, power) over the course of up to 2 weeks of
765 recordings (in the case of hM3Dq animals in which multiple doses of CNO or
766 vehicle were administered every 2 to 3 days). LFPs were then filtered using a
767 zero-phase offset filter in the theta (5-10 Hz), beta (14-18 Hz), low gamma (30-60
768 Hz) or high gamma (65-100 Hz) range. The Chronux function `mtspectrum`, a
769 multitaper spectral estimate, was used with 5 tapers, and resulting spectral
770 values were smoothed. For all treatments, spectral measures were made during
771 each of run and rest periods during the 30 to 60 minutes following treatment.
772 Spectral density plots for each behavioral state, each treatment and in each
773 recording site were averaged across animals according to genotype and AAV
774 infused. Peak powers in each frequency range were collected to compare
775 changes in peak theta, beta, low gamma or high gamma power according to
776 treatment. Cross frequency coupling of theta phase and low gamma (30-55 Hz)
777 power were also measured from hippocampal LFPs during periods of running
778 following each treatment using the method of ^{56,57}. Coherence measures were
779 performed using the Chronux function `cohgramc`⁵⁸, and mean low gamma
780 coherence was measured over the 30-60 Hz frequency range from the run and
781 rest subsets described above. Power and coherence values measured for each

782 treatment were compared using appropriate statistical tests, listed in text, after
783 data were checked for normal distributions and equal variance.

784

785 Ripple events were identified according to modified methods previously
786 described^{8,36} from recordings originating from the pyramidal cell layer during
787 periods of rest in hM3Dq (8 animals with dorsal CA1 recordings) and hM4Di (2
788 animals with dorsal CA1 recordings, 4 animals with intermediate CA1 recordings)
789 animals. These signals were denoised with an IIR notch filter at 60 and 180 Hz
790 and filtered between 100 and 300 Hz with a 69-order FIR zero phase shift filter.
791 Signals were then Hilbert transformed, and the absolute value envelopes were
792 smoothed with a 50-msec window. Envelope amplitude deflections that exceeded
793 3 standard deviations from the mean amplitude (i.e., mean +3 standard
794 deviations) for more than 30 msec were counted as ripple events. Deflections
795 within 200 msec of a previous ripple event excluded. Ripple event frequency and
796 ripple amplitude were measured and appropriate statistical tests were applied, as
797 listed in the text, after data were checked for normal distributions and equal
798 variance.

799

800 Behavioral measures

801 For all behavioral measures, the experimenter was blind to the genotype of
802 animals. Estrous cycle was not tracked in female mice. All behavioral assays
803 were performed during the light cycle, between 8 AM and 3 PM.

804

805 Two cohorts of *Amigo2-icreERT2* mice were tested for behavioral analyses. One
806 cohort was evaluated in assays for social approach, and another cohort was
807 evaluated in assays for prepulse inhibition of acoustic startle responses and
808 spontaneous alternation in a Y-maze. Between the time of performing the
809 acoustic startle response and spontaneous alternation assay, *Amigo2-icreERT2+*
810 and *Amigo2-icreERT2-* animals were removed from the group for histological
811 confirmation of hM4Di expression. For all assays, data were checked for normal
812 distribution and equal variance before choosing a statistical test. Estrous cycle
813 was not tracked in female mice. All behavioral assays were performed during the
814 light cycle, between 8 AM and 3 PM.

815

816 CNO treatment for behavioral assays: hM4Di AAV-infused *Amigo2-icreER* mice
817 undergoing behavioral studies were treated with 5 mg/kg CNO, IP, at specific
818 times stated below.

819

820 Social approach in a three-chamber choice test: CNO was administered 20
821 minutes before the beginning of the three-chamber test. Each session consisted
822 of two ten-minute phases: a habituation period and a test for sociability. For the
823 sociability assay, mice were given a choice between visiting a side of the
824 chamber with a novel sex-matched conspecific and visiting a side with no
825 conspecific in it. The social testing apparatus was a rectangular, three-
826 chambered box fabricated from clear Plexiglas (schematized in Fig. 7A). Dividing
827 walls had doorways allowed access into each chamber. An automated image

828 tracking system (Noldus Ethovision) provided measures of entries and duration in
829 each side of the social test box as well as time in spent within 5 cm of the
830 Plexiglass cages (the cage proximity zone). Times on each side are presented.

831

832 At the start of the test, the test mouse was placed in the middle chamber and
833 allowed to explore for ten minutes, with the doorways into the two side chambers
834 open. Measures of the amount of time spent in each side chamber were taken.
835 After this habituation period, the test mouse was enclosed in the center
836 compartment of the social test box, and an unfamiliar C57BL/6J “stranger” was
837 placed in one of the side chambers. The unfamiliar mouse was enclosed in a
838 small Plexiglass cage drilled with holes, which allowed nose contact, but
839 prevented fighting. An identical empty Plexiglass cage was placed in the opposite
840 side of the chamber. Following placement of the unfamiliar mouse in the empty
841 cage, the doors were re-opened, and the subject was allowed to explore the
842 entire social test box for a ten-minute session.

843

844 Prepulse Inhibition: Prepulse inhibition of acoustic startle responses, an index of
845 sensorimotor gating, was measured using an SR-LAB system (San Diego
846 Instruments, San Diego, CA). hM4Di AAV-infused animals were administered
847 CNO 30 minutes before beginning the prepulse inhibition assay. Mice were
848 placed inside the animal enclosure fitted to the size of the animal. The sound
849 proof chamber was then closed and the 20-min session begun. Background
850 white noise at 70 dB occurred throughout the session except during pre-pulse
851 and pulse stimuli. Pre-pulse stimuli were 73, 76 or 82 dB, 20 msec long, and
852 presented 100 msec before the pulse, which was 120 dB and 40 msec long.
853 Movements initiated by pulse stimuli were transduced into startle amplitude. A
854 session started with a 5-min acclimation period followed by three consecutive
855 blocks of trials. The first and last blocks consisted of six pulse-alone trials. The
856 middle block consisted of 52 pulse alone, prepulse+pulse, and no-stimulus
857 (background white noise only) trials in a pseudo-randomized order. The no-
858 stimulus trials were incorporated to measure basal movement of the animal.
859 Each trial was separated by a random, variable 15-sec inter-trial interval. Each
860 trial started with a 50 msec null period and ended with a 200 msec recording
861 period.

862

863 Spontaneous alternation: hM4Di AAV-infused mice were tested in the
864 spontaneous alternation task using a Y maze (Med Associates, consisting of
865 three 36.83 × 7.5 cm runways covered with removable clear Plexiglass). Red
866 lights at 3-5 lux illuminated the room, and visual cues were positioned on all four
867 walls at a height above the maze. At the start of a trial, the Plexiglass was
868 removed from the top of one arm of the Y-maze, a mouse was placed on a distal
869 end of the arm, and the Plexiglass was replaced. After a 10-sec delay, the door
870 separating the arm from the rest of the maze was opened, and the mouse was
871 allowed to explore the maze freely for 8 min. Trials were videotaped, and an
872 experimenter blind to the genotype scored entries of the mouse into arms during
873 the 8-min trial. Entry into an arm required all four limbs to be within the arm. An

874 alternation was scored when an animal entered three different arms sequentially.
875 Percent spontaneous alternation was calculated by dividing the number of
876 alternations by the maximum possible number of alternations as follows: (# of
877 alternations) / (total number of arm entries – 2).

878

879 Results Reporting and Data Availability

880 For each experiment presented within the Results section and in figures, the
881 number of replicates is presented as “N” when indicating the number of animals
882 that were used for the experiment or as “n” when referring to the number of
883 neurons used for the experiment. Statistical tests used for each experiment are
884 presented in the text. Statistical significance was based on a p-value of 0.05. All
885 error bars in graphs represent standard error of the mean. The data supporting
886 the findings of this study are available from the corresponding author upon
887 request.

888

889

890 **CONTRIBUTIONS:** G.M.A., L.Y.B., S.F., D.L., N.V.R., S.S.M., and S.M.D.
891 conceived of and designed the studies. G.M.A., L.Y.B., S.F., D.L., C.P., N.V.R.,
892 and P.J. conducted experiments and analyzed data. B.G. and N.W.P. generated
893 transgenic mice. G.M.A. and S.M.D. wrote the manuscript. S.S.M., P.J., and
894 S.M.D. supervised the project.

895

896 **ACKNOWLEDGEMENTS:** This research is supported by the Intramural
897 Research Program of the U.S. NIH, National Institute of Environmental Health
898 Sciences (Z01 ES100221 to S.M.D.). The UNC Mouse Behavioral Phenotyping
899 Laboratory is supported by U.S. NIH, National Institute of Child Health and
900 Human Development (U54HD079124 to Joseph Piven). We wish to thank
901 Guohong Cui, Jesse Cushman and the members of the Dudek lab for critically
902 reading this manuscript, as well as Jesse Cushman and the NIEHS
903 Neurobehavioral Core, the Fluorescence Microscopy and Imaging Center, and
904 the animal care staff at NIEHS for their support.

905

906 **REFERENCES**

- 907 1. Dudek, S. M., Alexander, G. M. & Farris, S. Rediscovering area CA2:
908 unique properties and functions. *Nat. Rev. Neurosci.* **17**, 89–102 (2016).
- 909 2. Alexander, G. M. *et al.* Social and novel contexts modify hippocampal CA2
910 representations of space. *Nature Communications* **7**, 10300 (2016).
- 911 3. Mankin, E. A., Diehl, G. W., Sparks, F. T., Leutgeb, S. & Leutgeb, J. K.
912 Hippocampal CA2 activity patterns change over time to a larger extent than
913 between spatial contexts. *Neuron* **85**, 190–201 (2015).
- 914 4. Lee, H., Wang, C., Deshmukh, S. S. & Knierim, J. J. Neural Population
915 Evidence of Functional Heterogeneity along the CA3 Transverse Axis:
916 Pattern Completion versus Pattern Separation. *Neuron* **87**, 1093–1105
917 (2015).
- 918 5. Lu, L., Igarashi, K. M., Witter, M. P., Moser, E. I. & Moser, M.-B.
919 Topography of Place Maps along the CA3-to-CA2 Axis of the
920 Hippocampus. *Neuron* **87**, 1078–1092 (2015).
- 921 6. Kay, K. *et al.* A hippocampal network for spatial coding during immobility
922 and sleep. *Nature* 1–26 (2016). doi:10.1038/nature17144
- 923 7. Oliva, A., Fernández-Ruiz, A., Buzsáki, G. & Berényi, A. Role of
924 Hippocampal CA2 Region in Triggering Sharp-Wave Ripples. *Neuron* **91**,
925 1342–1355 (2016).
- 926 8. Boehringer, R. *et al.* Chronic Loss of CA2 Transmission Leads to
927 Hippocampal Hyperexcitability. *Neuron* **94**, 642–655.e9 (2017).
- 928 9. Colgin, L. L. *et al.* Frequency of gamma oscillations routes flow of
929 information in the hippocampus. *Nature* **462**, 353–357 (2009).
- 930 10. Schomburg, E. W. *et al.* Theta phase segregation of input-specific gamma
931 patterns in entorhinal-hippocampal networks. *Neuron* **84**, 470–485 (2014).
- 932 11. Bragin, A. *et al.* Gamma (40–100 Hz) oscillation in the hippocampus of the
933 behaving rat. *J. Neurosci.* **15**, 47–60 (1995).
- 934 12. Zheng, C., Wood Bieri, K., Hwaun, E. & Lee Colgin, L. Fast Gamma
935 Rhythms in the Hippocampus Promote Encoding of Novel Object-Place
936 Pairings. *eNeuro* **3**, 1–19 (2016).
- 937 13. Kemere, C., Carr, M. F., Karlsson, M. P. & Frank, L. M. Rapid and
938 continuous modulation of hippocampal network state during exploration of
939 new places. *PLoS ONE* **8**, e73114 (2013).
- 940 14. Colgin, L. L. Do slow and fast gamma rhythms correspond to distinct
941 functional states in the hippocampal network? *Brain Res.* 1–7 (2015).
942 doi:10.1016/j.brainres.2015.01.005
- 943 15. Tort, A. B. L., Komorowski, R. W., Manns, J. R., Kopell, N. J. &
944 Eichenbaum, H. Theta-gamma coupling increases during the learning of
945 item-context associations. *Proc. Natl. Acad. Sci. U.S.A.* **106**, 20942–20947
946 (2009).
- 947 16. Shirvalkar, P. R., Rapp, P. R. & Shapiro, M. L. Bidirectional changes to
948 hippocampal theta-gamma comodulation predict memory for recent spatial
949 episodes. *Proc. Natl. Acad. Sci. U.S.A.* **107**, 7054–7059 (2010).
- 950 17. Middleton, S. J. & McHugh, T. J. Silencing CA3 disrupts temporal coding in
951 the CA1 ensemble. *Nat Neurosci* 1–10 (2016). doi:10.1038/nn.4311

- 952 18. Buzsáki, G., Horváth, Z., Urioste, R., Hetke, J. & Wise, K. High-frequency
953 network oscillation in the hippocampus. *Science* **256**, 1025–1027 (1992).
- 954 19. Ylinen, A. *et al.* Sharp wave-associated high-frequency oscillation (200 Hz)
955 in the intact hippocampus: network and intracellular mechanisms. *J.*
956 *Neurosci.* **15**, 30–46 (1995).
- 957 20. Hitti, F. L. & Siegelbaum, S. A. The hippocampal CA2 region is essential
958 for social memory. *Nature* 1–17 (2014). doi:10.1038/nature13028
- 959 21. Pagani, J. H. *et al.* Role of the vasopressin 1b receptor in rodent
960 aggressive behavior and synaptic plasticity in hippocampal area CA2. *Mol.*
961 *Psychiatry* 1–10 (2014). doi:10.1038/mp.2014.47
- 962 22. Smith, A. S., Williams Avram, S. K., Cymerblit-Sabba, A., Song, J. &
963 Young, W. S. Targeted activation of the hippocampal CA2 area strongly
964 enhances social memory. *Mol. Psychiatry* **21**, 1137–1144 (2016).
- 965 23. Piskorowski, R. A. *et al.* Age-Dependent Specific Changes in Area CA2 of
966 the Hippocampus and Social Memory Deficit in a Mouse Model of the
967 22q11.2 Deletion Syndrome. *Neuron* **89**, 163–176 (2016).
- 968 24. Sigurdsson, T., Stark, K. L., Karayiorgou, M., Gogos, J. A. & Gordon, J. A.
969 Impaired hippocampal-prefrontal synchrony in a genetic mouse model of
970 schizophrenia. *Nature* **464**, 763–767 (2010).
- 971 25. Armbruster, B. N., Li, X., Pausch, M. H., Herlitze, S. & Roth, B. L. Evolving
972 the lock to fit the key to create a family of G protein-coupled receptors
973 potently activated by an inert ligand. *Proc. Natl. Acad. Sci. U.S.A.* **104**,
974 5163–5168 (2007).
- 975 26. Alexander, G. M. *et al.* Remote control of neuronal activity in transgenic
976 mice expressing evolved G protein-coupled receptors. *Neuron* **63**, 27–39
977 (2009).
- 978 27. Madisen, L. *et al.* A robust and high-throughput Cre reporting and
979 characterization system for the whole mouse brain. *Nat Neurosci* **13**, 133–
980 140 (2010).
- 981 28. Kohara, K. *et al.* Cell type-specific genetic and optogenetic tools reveal
982 hippocampal CA2 circuits. *Nature Publishing Group* **17**, 269–279 (2014).
- 983 29. Spellman, T. *et al.* Hippocampal-prefrontal input supports spatial encoding
984 in working memory. *Nature* **522**, 309–314 (2015).
- 985 30. Thierry, A. M., Gioanni, Y., Dégénétais, E. & Glowinski, J. Hippocampo-
986 prefrontal cortex pathway: anatomical and electrophysiological
987 characteristics. *Hippocampus* **10**, 411–419 (2000).
- 988 31. Swanson, L. W. A direct projection from Ammon's horn to prefrontal cortex
989 in the rat. *Brain Res.* **217**, 150–154 (1981).
- 990 32. Stachniak, T. J., Ghosh, A. & Sternson, S. M. Chemogenetic Synaptic
991 Silencing of Neural Circuits Localizes a Hypothalamus→Midbrain Pathway
992 for Feeding Behavior. *Neuron* (2014). doi:10.1016/j.neuron.2014.04.008
- 993 33. Tamamaki, N., Abe, K. & Nojyo, Y. Three-dimensional analysis of the
994 whole axonal arbors originating from single CA2 pyramidal neurons in the
995 rat hippocampus with the aid of a computer graphic technique. *Brain Res.*
996 **452**, 255–272 (1988).
- 997 34. Jay, T. M. & Witter, M. P. Distribution of hippocampal CA1 and subicular

- 998 efferents in the prefrontal cortex of the rat studied by means of anterograde
999 transport of Phaseolus vulgaris-leucoagglutinin. *J. Comp. Neurol.* **313**,
1000 574–586 (1991).
- 1001 35. Jay, T. M., Glowinski, J. & Thierry, A. M. Selectivity of the hippocampal
1002 projection to the prelimbic area of the prefrontal cortex in the rat. *Brain*
1003 *Res.* **505**, 337–340 (1989).
- 1004 36. Suh, J., Foster, D. J., Davoudi, H., Wilson, M. A. & Tonegawa, S. Impaired
1005 hippocampal ripple-associated replay in a mouse model of schizophrenia.
1006 *Neuron* **80**, 484–493 (2013).
- 1007 37. Arguello, P. A. & Gogos, J. A. Modeling madness in mice: one piece at a
1008 time. *Neuron* **52**, 179–196 (2006).
- 1009 38. Whittington, M. A., Traub, R. D. & Jefferys, J. G. Synchronized oscillations
1010 in interneuron networks driven by metabotropic glutamate receptor
1011 activation. *Nature* **373**, 612–615 (1995).
- 1012 39. Fisahn, A., Pike, F. G., Buhl, E. H. & Paulsen, O. Cholinergic induction of
1013 network oscillations at 40 Hz in the hippocampus in vitro. *Nature* **394**, 186–
1014 189 (1998).
- 1015 40. Mann, E. O., Suckling, J. M., Hajos, N., Greenfield, S. A. & Paulsen, O.
1016 Perisomatic feedback inhibition underlies cholinergically induced fast
1017 network oscillations in the rat hippocampus in vitro. *Neuron* **45**, 105–117
1018 (2005).
- 1019 41. Lee, S.-H. *et al.* Parvalbumin-Positive Basket Cells Differentiate among
1020 Hippocampal Pyramidal Cells. *Neuron* **82**, 1129–1144 (2014).
- 1021 42. Mercer, A., Eastlake, K., Trigg, H. L. & Thomson, A. M. Local circuitry
1022 involving parvalbumin-positive basket cells in the CA2 region of the
1023 hippocampus. *Hippocampus* **22**, 43–56 (2010).
- 1024 43. Valero, M. *et al.* Determinants of different deep and superficial CA1
1025 pyramidal cell dynamics during sharp-wave ripples. *Nat Neurosci* 1–14
1026 (2015). doi:10.1038/nn.4074
- 1027 44. Berke, J. D., Hetrick, V., Breck, J. & Greene, R. W. Transient 23-30 Hz
1028 oscillations in mouse hippocampus during exploration of novel
1029 environments. *Hippocampus* **18**, 519–529 (2008).
- 1030 45. Grossberg, S. Beta oscillations and hippocampal place cell learning during
1031 exploration of novel environments. *Hippocampus* **19**, 881–885 (2009).
- 1032 46. Wintzer, M. E., Boehringer, R., Polygalov, D. & McHugh, T. J. The
1033 Hippocampal CA2 Ensemble Is Sensitive to Contextual Change. *J.*
1034 *Neurosci.* **34**, 3056–3066 (2014).
- 1035 47. Wersinger, S. R., Ginns, E. I., O'Carroll, A.-M., Lolait, S. J. & Young, W. S.,
1036 III. Vasopressin V1b receptor knockout reduces aggressive behavior in
1037 male mice. *Mol. Psychiatry* **7**, 975–984 (2002).
- 1038 48. Bartesaghi, R. & Ravasi, L. Pyramidal neuron types in field CA2 of the
1039 guinea pig. *Brain Res. Bull.* **50**, 263–273 (1999).
- 1040 49. Woo, T.-U. W., Spencer, K. & McCarley, R. W. Gamma oscillation deficits
1041 and the onset and early progression of schizophrenia. *Harv Rev Psychiatry*
1042 **18**, 173–189 (2010).
- 1043 50. Pinkham, A. E., Hopfinger, J. B., Pelphrey, K. A., Piven, J. & Penn, D. L.

- 1044 Neural bases for impaired social cognition in schizophrenia and autism
1045 spectrum disorders. *Schizophr. Res.* **99**, 164–175 (2008).
- 1046 51. Benes, F. M., Kwok, E. W., Vincent, S. L. & Todtenkopf, M. S. A reduction
1047 of nonpyramidal cells in sector CA2 of schizophrenics and manic
1048 depressives. *Biol. Psychiatry* **44**, 88–97 (1998).
- 1049 52. Beasley, C. L. & Reynolds, G. P. Parvalbumin-immunoreactive neurons are
1050 reduced in the prefrontal cortex of schizophrenics. *Schizophr. Res.* **24**,
1051 349–355 (1997).
- 1052 53. Hainer, C. *et al.* Beyond Gene Inactivation: Evolution of Tools for Analysis
1053 of Serotonergic Circuitry. *ACS Chem Neurosci* **6**, 1116–1129 (2015).
- 1054 54. Lee, E. C. *et al.* A highly efficient Escherichia coli-based chromosome
1055 engineering system adapted for recombinogenic targeting and subcloning
1056 of BAC DNA. *Genomics* **73**, 56–65 (2001).
- 1057 55. Skaggs, W. E., McNaughton, B. L., Wilson, M. A. & Barnes, C. A. Theta
1058 phase precession in hippocampal neuronal populations and the
1059 compression of temporal sequences. *Hippocampus* **6**, 149–172 (1996).
- 1060 56. Tort, A. B. L. *et al.* Dynamic cross-frequency couplings of local field
1061 potential oscillations in rat striatum and hippocampus during performance
1062 of a T-maze task. *Proc. Natl. Acad. Sci. U.S.A.* **105**, 20517–20522 (2008).
- 1063 57. Tort, A. B. L., Komorowski, R., Eichenbaum, H. & Kopell, N. Measuring
1064 phase-amplitude coupling between neuronal oscillations of different
1065 frequencies. *J. Neurophysiol.* **104**, 1195–1210 (2010).
- 1066 58. Bokil, H., Andrews, P., Kulkarni, J. E., Mehta, S. & Mitra, P. P. Chronux: a
1067 platform for analyzing neural signals. *J. Neurosci. Methods* **192**, 146–151
1068 (2010).
- 1069
- 1070

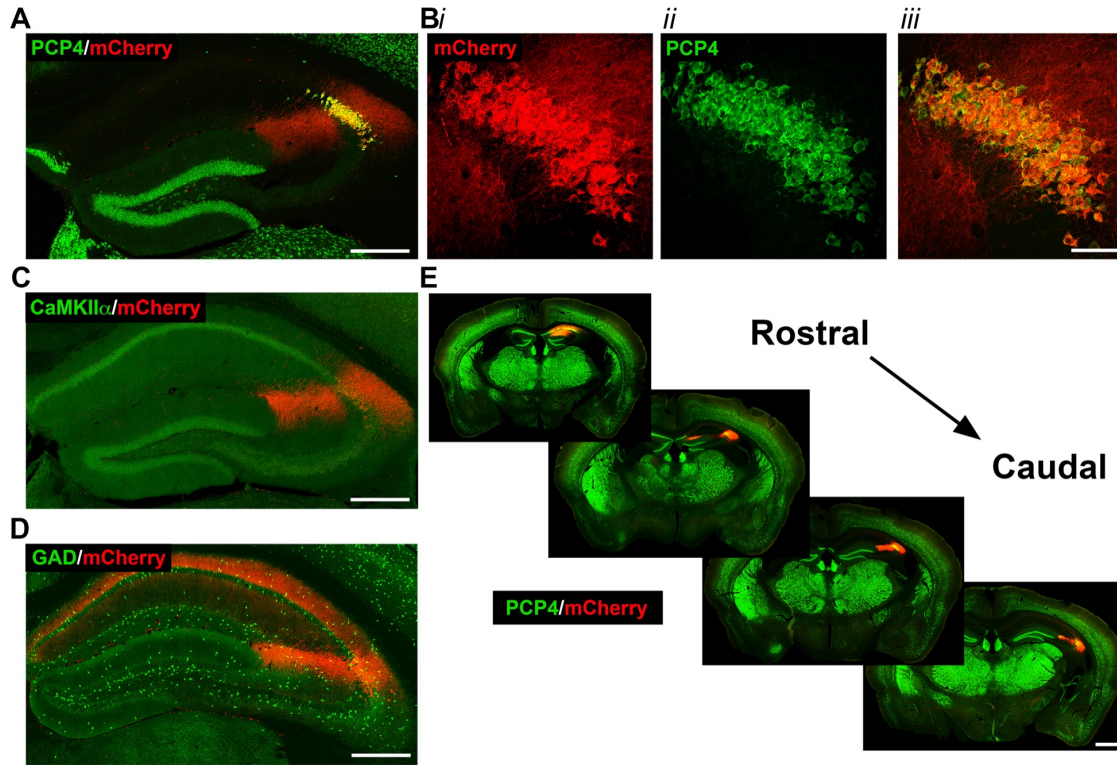


Figure 1.

1071
1072
1073
1074
1075
1076
1077
1078
1079
1080
1081
1082
1083
1084
1085
1086
1087

Figure 1. Selective expression of mCherry-tagged DREADD receptors in CA2 pyramidal cells of *Amigo2-icreERT2* mice. Coronal sections from *Amigo2-icreERT2*⁺ mice infused unilaterally with AAV-hSyn-DIO-hM3D(Gq)-mCherry (hM3Dq AAV; A-C,E) or bilaterally with AAV-hSyn-DIO-hM4D(Gi)-mCherry (hM4Di AAV; D) and treated with tamoxifen. A-B. Expression of hM3Dq-mCherry and the CA2-specific marker PCP4, in the hippocampus (A) and CA2 (B). In B, *i* shows DREADD-mCherry expression, *ii* shows PCP4 expression and *iii* shows the merged image. Expression of DREADD-mCherry colocalizes with CaMKII α , a marker for principal neurons in hippocampus (C), but does not colocalize with GAD, a marker for inhibitory neurons (D). Note that hM4Di-mCherry (shown in D) fills axons projecting to CA1. (E) Expression of hM3Dq-mCherry colocalizes with expression of PCP4 across the rostral to caudal extent of CA2. Scale bars = 200 μ m (A, C, D), 50 μ m (B) and 1 mm (E).

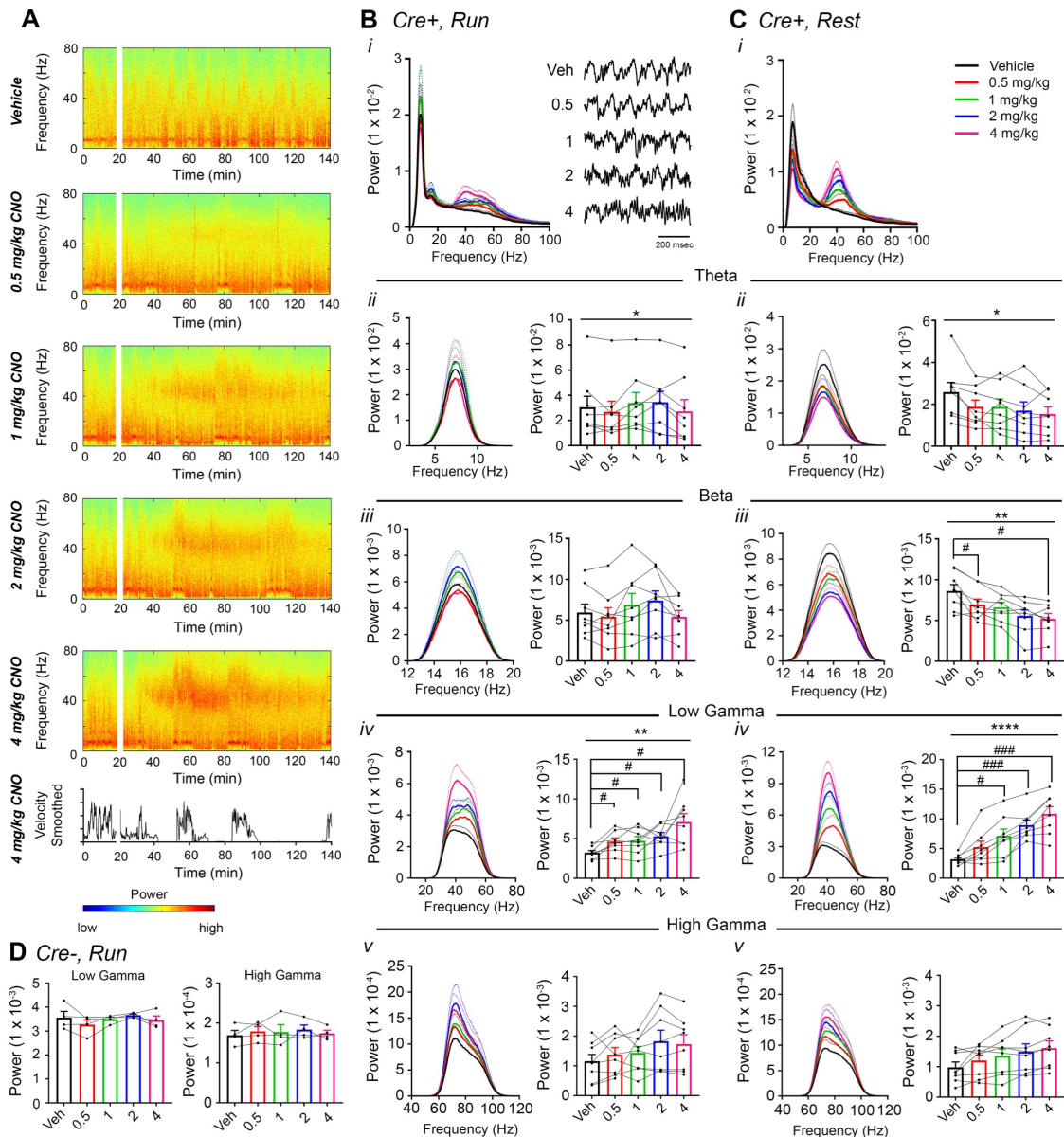


Figure 2.

1088

1089

1090

1091 **Figure 2.** CNO treatment dose-dependently increases low gamma power in

1092 hippocampus of hM3Dq-infused *Amigo2-icreERT2+* mice. (A) Spectrograms of

1093 hippocampal LFP recordings depicting LFP power according to different

1094 frequencies over time. Vehicle/CNO administration time is shown by the white

1095 bar, and the treatment is shown to the left of each spectrogram. Locomotor

1096 velocity is shown in the bottom panel, corresponding to the 4 mg/kg CNO

1097 spectrogram. (B-C) Power measures for hippocampal LFPs in *Amigo2-*

1098 *icreERT2+* mice during periods of running (B) and resting (C). For each of B and

1099 (i-v) Power spectral density plots and peak power from LFPs filtered in the theta

1100 (5-10 Hz; *ii*), beta (14-18 Hz; *iii*), low gamma (30-60 Hz; *iv*), or high gamma (65-
1101 100 Hz; *v*) frequency ranges. In *Bi*, raw LFP traces are shown to the right of the
1102 power spectral density plot for each treatment, sampled during a period of
1103 running during the 30-60 minutes following treatment listed. In *Bii-v* and *Cii-v*,
1104 plots on the left show power spectral density plots for each frequency band, and
1105 plots on the right show mean peak power for the population of animals in colored
1106 bars and data from individual animals as black dots. (*Bii*) Theta power varied
1107 significantly upon treatment during running (N=8 mice (3 female, 5 male);
1108 Friedman statistic=11.3; $p=0.0234$, results of *post hoc* tests not significant). *B(iii)*
1109 CNO treatment did not significantly affect beta power (F(2.274, 15.91)=2.91,
1110 $p=0.0784$, repeated-measures one-way ANOVA with Geisser-Greenhouse
1111 correction for unequal variance). (*Biv*) CNO treatment produced a significant
1112 dose-dependent increase in low gamma power during running (F(1.904,
1113 13.33)=9.457, $p=0.0030$, repeated-measures one-way ANOVA with Geisser-
1114 Greenhouse correction for unequal variance; results of Holm-Sidak *post hoc*
1115 tests are shown by symbols. (*Bv*) CNO treatment did not significantly affect high
1116 gamma power during running (F(1.384, 9.69)=2.288, $p=0.1602$, repeated-
1117 measures one-way ANOVA with Geisser-Greenhouse correction for unequal
1118 variance). (*Cii*) Theta power varied significantly upon treatment during rest (same
1119 N; F(1.972, 13.81)=4.825, $p=0.0261$, repeated-measures one-way ANOVA with
1120 Geisser-Greenhouse correction for unequal variance; results of *post hoc* tests
1121 not significant). (*Ciii*) CNO treatment produced a significant decrease in beta
1122 power during rest (F(1.408, 9.857)=10.07, $p=0.0066$, repeated-measures one-
1123 way ANOVA with Geisser-Greenhouse correction for unequal variance; results of
1124 Holm-Sidak *post hoc* tests are shown by symbols. (*Civ*) CNO treatment produced
1125 a significant dose-dependent increase in low gamma power during rest (F(2.306,
1126 16.15)=32.2), $p<0.0001$, repeated-measures one-way ANOVA with Geisser-
1127 Greenhouse correction for unequal variance; results of Holm-Sidak *post hoc*
1128 tests are shown by symbols). (*Cv*) CNO treatment did not significantly affect high
1129 gamma power during rest (F(1.286, 9.003)=4.775, $p=0.0501$, repeated-measures
1130 one-way ANOVA with Geisser-Greenhouse correction for unequal variance). (D)
1131 Peak low gamma (left plot) and high gamma (right plot) power for the population
1132 of *Amigo2-icreERT2-* mice infused with hM3Dq, treated with tamoxifen and
1133 challenged with CNO. Neither low gamma power nor high gamma power
1134 changed significantly in response to CNO administration during running (N=4
1135 male mice; low gamma: F(1.669, 5.006)=1.36, $p=0.3281$; high gamma: F(1.895,
1136 5.684)=0.5079, $p=0.6175$, repeated-measures one-way ANOVA with Geisser-
1137 Greenhouse correction for unequal variance). * $p<0.05$, ** $p<0.01$, **** $p<0.0001$,
1138 one-way ANOVA; # $p<0.05$, ### $p<0.001$, Holm-Sidak *post hoc* test.

1139
1140

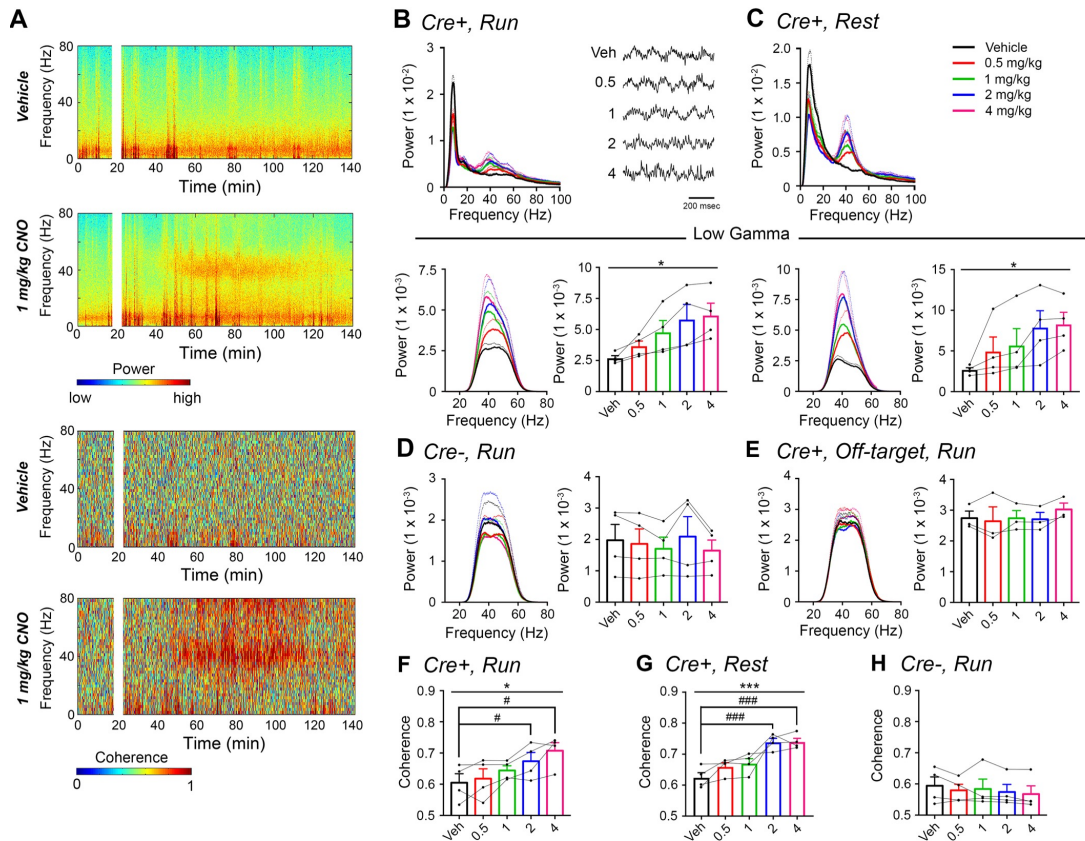


Figure 3.

1141
1142
1143
1144
1145
1146
1147
1148
1149
1150
1151
1152
1153
1154
1155
1156
1157
1158
1159
1160
1161
1162

Figure 3. CNO treatment dose-dependently increases low gamma power in PFC of hM3Dq-infused *Amigo2-icreERT2+* mice. (A) Spectrograms of PFC LFP recordings depicting power (top two panels) and coherograms depicting coherence between PFC and hippocampal LFP recordings (bottom two panels) according to different frequencies over time. Vehicle/CNO (1 mg/kg, SQ) administration time is shown by the white bar, and the treatment is shown to the left of each spectrogram. (B-C) Power measures for PFC LFPs during periods of running (B) and resting (C) for *Amigo2-icreERT2+* mice. For each of B and C: Top plots show power spectral densities of LFPs for frequencies up to 100 Hz and bottom plots show power measured from PFC LFPs filtered in the low gamma (30-60 Hz) frequency range for each of run and rest periods. LFP traces in B show example LFPs during periods of running following the listed treatment. CNO treatment significantly increased low gamma power during both running (N=4 mice (3 male, 1 female); $F(1.168, 3.505)=9.146$, $p=0.0450$, repeated-measures one-way ANOVA with Geisser-Greenhouse correction for unequal variance; results of Holm-Sidak *post hoc* tests not significant) and resting ($F(1.561, 4.684)=7.155$, $p=0.0409$, repeated-measures one-way ANOVA with Geisser-Greenhouse correction for unequal variance). (D) Mean gamma power spectra and peak gamma power recorded from PFC for the population of hM3Dq infused *Amigo2-icreERT2-* mice during periods of running. Low gamma power

1163 did not significantly change in *Amigo2-icreERT2-* mice upon CNO administration
1164 (N=4 male mice; $F(1.349, 4.047)=1.809$, $p=0.2617$; repeated-measures one-way
1165 ANOVA with Geisser-Greenhouse correction for unequal variance). (E) Mean low
1166 gamma power spectra and peak low gamma power for recordings from *Amigo2-*
1167 *icreERT2+* mice infused with hM3Dq in which recording wires missed the target
1168 PFC area. CNO administration produced no significant change in peak low
1169 gamma power from off-target recordings (N=3 mice (1 male, 2 female); $F(1.742,$
1170 $3.483)=0.7609$, $p=0.5145$; repeated-measures one-way ANOVA with Geisser-
1171 Greenhouse correction for unequal variance). Each of the animals used for data
1172 shown in E showed increased low gamma power in hippocampus upon CNO
1173 administration. (F-G) Mean coherence between PFC and hippocampal low
1174 gamma-filtered LFPs during periods of run (F) and rest (G) for *Amigo2-*
1175 *icreERT2+* mice successfully targeted to PFC. CNO treatment produced a
1176 significant increase in low gamma coherence between hippocampus and PFC
1177 during both running (N=4 mice; $F(1.595, 4.786)=8.279$, $p=0.0305$; repeated-
1178 measures one-way ANOVA with Geisser-Greenhouse correction for unequal
1179 variance, results of Holm-Sidak *post hoc* tests shown by symbols) and resting
1180 ($F(4, 12)=11.71$, $p=0.0004$; repeated-measures one-way ANOVA, results of
1181 Holm-Sidak *post hoc* tests shown by symbols). (H) *Amigo2-icreERT2-* animals
1182 showed no significant change in low gamma coherence upon CNO
1183 administration (N=4 male mice; $F(4, 12)=1.053$, $p=0.4209$; repeated-measures
1184 one-way ANOVA). All spectral plots show mean spectra for the population of
1185 animals with colors representing treatments. Bar graphs show mean peak
1186 gamma power (B-E) or mean gamma coherence (F-H) for the population of
1187 animals in colored bars according to treatment and data from individual animals
1188 in black dots. Dotted lines on spectral plots and error bars on bar graphs
1189 represent standard error of the mean. * $p<0.05$, *** $p<0.001$, one-way ANOVA;
1190 # $p<0.05$, ### $p<0.001$, Holm-Sidak *post hoc* test.
1191
1192
1193

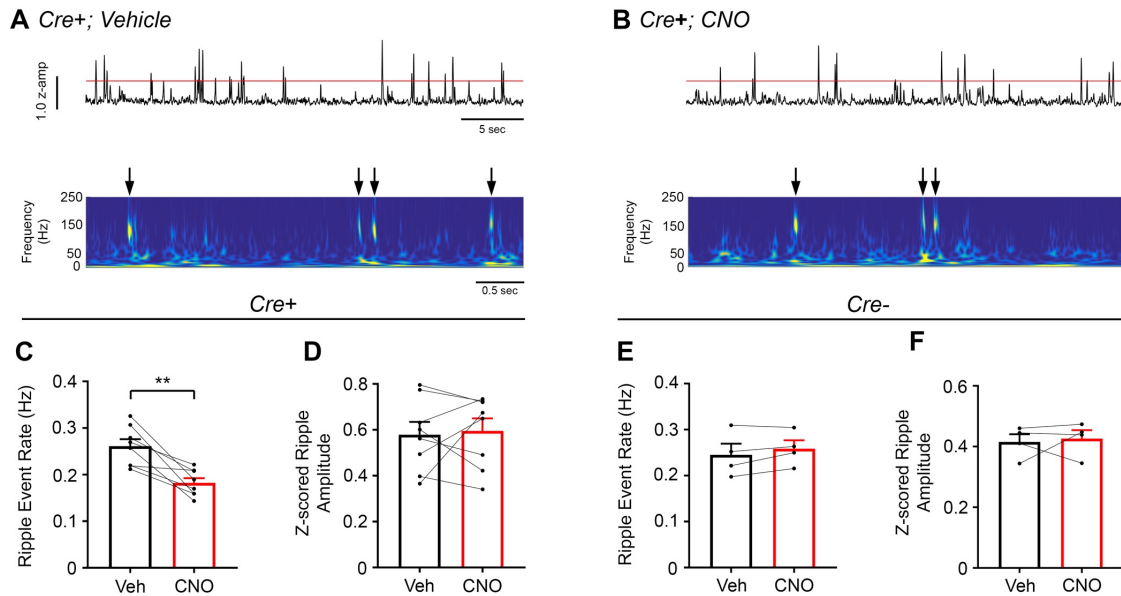
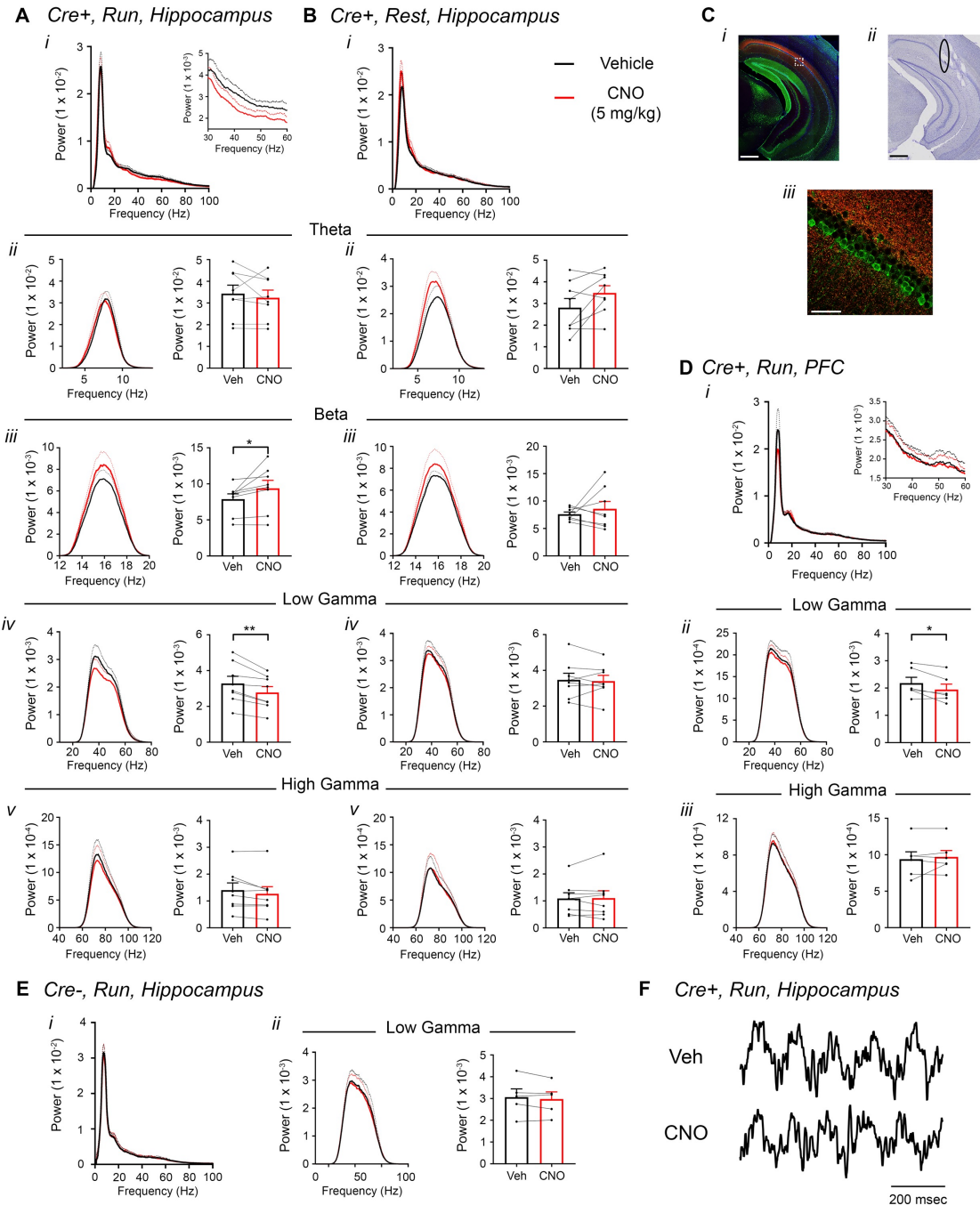


Figure 4.

1194
1195
1196
1197
1198
1199
1200
1201
1202
1203
1204
1205
1206
1207
1208
1209
1210
1211

Figure 4. Chemoactivation of CA2 pyramidal cells with hM3Dq decreases high-frequency ripple event rate. (A) Envelopes of ripple-filtered CA1 LFPs (top) recorded during periods of rest following administration of vehicle (left) or CNO (right; 0.5 mg/kg, SQ) and wavelet-filtered spectrograms (bottom) of the same LFPs. Cooler colors represent low power and warmer colors represent high power. Arrows denote examples of ripples shown by spectrogram. (C-D) Ripple event rate (C) but not amplitude (D) was significantly decreased in hM3Dq-expressing mice following CNO administration compared to that following vehicle administration (Ripple event rate: N=8 mice (5 male, 3 female); $t(7)=4.574$, $p=0.0026$; two-tailed paired t-test; Amplitude: $t(7)=0.3004$, $p=0.7726$, two-tailed paired t-test). (E-F) Ripple event rate and amplitude were not significantly changed in *Amigo2-icreERT2*-hM3Dq-infused mice (Ripple event rate: N=4 male mice, $t(3)=1.871$, $p=0.1581$, two-tailed paired t-test; Amplitude: N=4 male mice, $t(3)=0.3193$, $p=0.7704$, two-tailed paired t-test). ** $p<0.01$.



1212
1213
1214
1215
1216
1217
1218
1219
1220

Figure 5. Inhibition of CA2 pyramidal cells with hM4Di decreases hippocampal and PFC low gamma power. (A-B) Hippocampal LFP power measures from *Amigo2-icreERT2+* mice infused with hM4Di AAV and treated with vehicle or CNO (5 mg/kg, SQ; LFP samples 30-60 minutes following treatment) during periods of running (A) and resting (B). For each of A and B: (i) Power spectral density plots from raw LFPs for frequencies up to 100 Hz. Inset plot in Ai is expanded from Ai. (ii-v) Power spectral density plots and peak power measured

1221 in the theta (5-10 Hz; *ii*), beta (14-18 Hz; *iii*), low gamma (30-60 Hz; *iv*) or high
1222 gamma (65-100 Hz; *v*) frequency ranges. In *Aii-v* and *Bii-v*, plots on the left show
1223 power spectral density for the listed frequency bands, and plots on the right show
1224 mean peak power for the population of animals in colored bars according to
1225 treatment and dots representing data from individual animals. (*Aiii*) CNO
1226 administration produced a significant increase in beta power during running (N=8
1227 mice (4 female, 4 male); $t(7)=2.401$, $p=0.0474$, two-tailed paired t-test. (*Aiv*) CNO
1228 administration produced a significant decrease in hippocampal low gamma
1229 power during running (same N; $t(7)=4.408$, $p=0.0031$, two-tailed paired t-test).
1230 CNO treatment did not affect theta power during running ($t(7)=0.7786$, $p=0.4617$;
1231 *Aii*), high gamma power during running ($t(7)=2.029$, $p=0.0821$; *Av*), theta power
1232 during rest ($t(7)=2.214$, $p=0.0625$; *Bii*), beta power during rest ($t(7)=0.7453$,
1233 $p=0.0625$; *Biii*), low gamma power during rest ($t(7)=0.4522$, $p=0.6648$; *Biv*) or
1234 high gamma power during rest ($t(7)=0.172$, $p=0.8683$; *Bv*). (C) Expression of
1235 mCherry-tagged hM4Di in intermediate CA1 and electrode tracks at a similar
1236 position. (*Ci*) Expression of mCherry-tagged hM4Di (red) and calbindin (green) in
1237 an intermediate hippocampal section. The white box shows the area that is
1238 expanded in *Ciii*. Axons expressing hM4Di target intermediate CA1, with
1239 preferential targeting toward *stratum oriens*. (*Cii*) Electrode tracks of intermediate
1240 CA1 recording wires (black ellipse surrounds one of the tracks). (D) PFC LFP
1241 power measures from same mice used in A-B. (*i*) Power spectral density plots
1242 from raw LFPs for frequencies up to 100 Hz. Inset plot is expanded from the
1243 adjacent plot. (*ii-iii*) Power spectral density plot and peak power measured from
1244 low gamma (*ii*) and high gamma (*iii*) filtered LFPs. CNO administration produced
1245 a significant decrease in PFC low gamma power during running (N=6 mice (3
1246 female, 3 male); $t(5)=2.948$, $p=0.0320$, two-tailed paired t-test) but did not affect
1247 PFC high gamma power ($t(5)=0.738$, $p=0.4937$). (E) Power spectral density plot
1248 for the population of *Amigo2-icreERT2-* mice infused with hM3Di, treated with
1249 tamoxifen and challenged with CNO. Plots show spectral density of frequencies
1250 below 100 Hz (*i*), low gamma-filtered LFP spectral power and peak low gamma
1251 power for the population of animals (*ii*). CNO administration did not significantly
1252 affect low gamma power in *Amigo2-icreERT2-* mice during running (N=5 male
1253 mice; $t(4)=1.079$, $p=0.3413$; two-tailed paired t-test). (F) Example LFP traces
1254 from periods of running following vehicle or CNO treatment. * $p<0.05$, ** $p<0.01$.
1255 Scale bars = 500 μm (*Ci, ii*) and 75 μm (*Ciii*).

1256
1257
1258
1259
1260
1261
1262

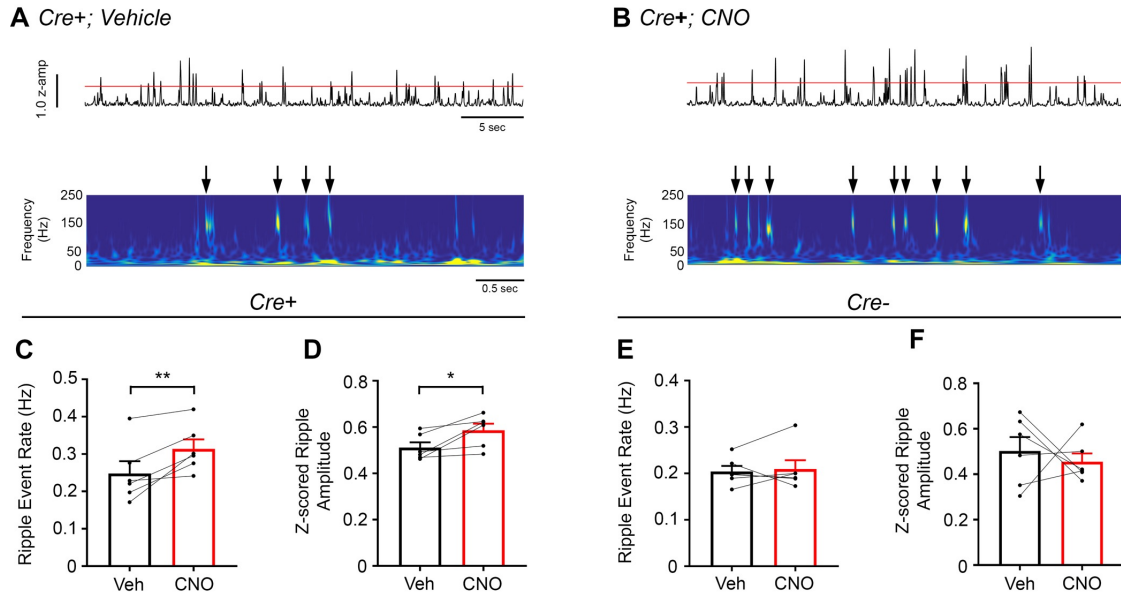


Figure 6.

1263
1264
1265
1266
1267
1268
1269
1270
1271
1272
1273
1274
1275
1276
1277
1278
1279
1280
1281
1282
1283
1284
1285
1286
1287
1288
1289
1290

Figure 6. Inhibition of CA2 pyramidal cells with hM4Di increases high-frequency ripple event rate and amplitude. (A) Envelopes of ripple-filtered CA1 LFPs (top) recorded during periods of rest following administration of vehicle (left) or CNO (right; 5 mg/kg, SQ) and wavelet-filtered spectrograms (bottom) of the same LFPs. Cooler colors represent low power and warmer colors represent high power. Arrows denote examples of ripples shown by spectrogram. (C-D) Ripple event rate (C) and amplitude (D) were significantly increased in hM4Di-expressing mice following CNO treatment compared to that following vehicle treatment (Ripple event rate: N=6 mice (3 male, 3 female); $t(5)=3.809$, $p=0.0063$; two-tailed paired t-test; Amplitude: N=6; $t(5)=3.069$, $p=0.0278$, two-tailed paired t-test). (E-F) Ripple event rate and amplitude were not significantly changed in *Amigo2-icreERT2*-hM4Di-infused mice (Ripple event rate: N=6 male mice; $W=5$, $p=0.6875$, Wilcoxon signed-ranked test; Amplitude: $t(5)=0.5165$, $p=0.6275$, two-tailed paired t-test). * $p<0.05$, ** $p<0.01$.

1291

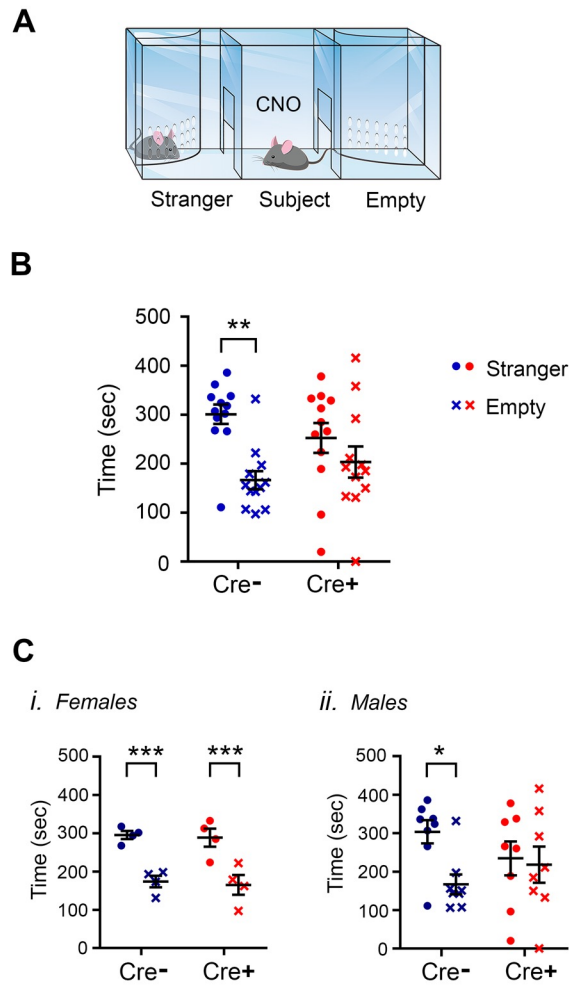


Figure 7.

1292

1293

1294 **Figure 7.** Inhibition of CA2 pyramidal cells with hM4Di decreases social

1295 approach behaviors. (A) Schematic diagram of three-chamber social approach

1296 chamber used for this study. CNO (5 mg/kg, IP) was administered to the all

1297 subject mice 20 min before starting the experiment. (B) *Amigo2-icreERT2-*, but

1298 not *Amigo2-icreERT2+*, hM4Di-expressing mice spent significantly more time in

1299 the social chamber than the empty chamber in the social approach assay (male

1300 (8 Cre+ and 8 Cre-) and female (4 Cre+ and 4 Cre-) mice combined; main effect of chamber: $F(1, 22)=9.852, p=0.0048$; main effect of genotype: $F(1,$

1301 $22)=0.06729, p=0.7977$, repeated measures two-way ANOVA; Cre+ time spent in

1302 social chamber versus empty chamber: $F(1, 11)=1.15; p=0.3057$; Cre- time spent in

1303 social chamber versus empty chamber: $F(1, 11)=13.52; p=0.0037$, within-

1304 genotype repeated measures ANOVAs). (C) Social approach data shown for

1305 females (i) and males (ii) separately. (i) Female Cre+ hM4Di-expressing mice

1306 showed similar preference for the social chamber as Cre- mice (N=8 female mice

1307 (4 pairs); main effect of chamber: $F(1,6)=106.6$, $p<0.0001$; main effect of
1308 genotype: $F(1,6)=0.001545$, $p=0.9699$, repeated measures two-way ANOVA;
1309 Cre+ time spent in social chamber versus empty chamber: $p=0.0005$; Cre- time
1310 spent in social chamber versus empty chamber: $p=0.0002$, within-genotype
1311 repeated measures ANOVA). (ii). Male Cre+ hM4Di-expressing mice did not
1312 show a preference for the social chamber, while Cre- mice did (N=16 male mice
1313 (8 Cre+ and 8 Cre- mice); main effect of chamber: $F(1,14)=3.123$, $p=0.0990$;
1314 main effect of genotype: $F(1,14)=0.08210$, $p=0.7787$, repeated measures two-
1315 way ANOVA; Cre+ time spent in social chamber versus empty chamber:
1316 $p=0.7932$; Cre- time spent in social chamber versus empty chamber: $p=0.0425$,
1317 within-genotype repeated measures ANOVA). Each dot represents data from an
1318 individual animal, and black horizontal lines and error bars represent means and
1319 standard errors of the mean.
1320
1321
1322
1323
1324
1325
1326